UPPER-MANTLE VELOCITY STRUCTURE BENEATH THE WESTERN PHILIPPINE SEA PLATE FROM BODY WAVES, SURFACE WAVES, AND *SCS* REVERBERATIONS

by

MAMORU KATO

B.S., Geophysics, Kyoto University, 1990
M.S., Geophysics, Kyoto University, 1992

Submitted to the Department of
Earth, Atmospheric, and Planetary Sciences
in partial fulfillment of the requirements for the degree of

MASTER OF SCIENCE IN GEOPHYSICS

at the

MASSACHUSETTS INSTITUTE OF TECHNOLOGY

February, 1996

Signature of Author _____
Department of Earth, Atmospheric, and Planetary Sciences
January 1996

Certified by _____
Thomas H. Jordan
Thesis Supervisor

Accepted by _____
Thomas H. Jordan
Department Head

Abstract

The seismic structure of the western Philippine Sea corridor, which samples major back-arc basins, has been investigated by two sets of seismological observations. *ScS* reverberation data provides vertical travel times to and shear impedance across the major discontinuities, which gives a framework for a regional upper mantle model, and our observations of frequency-dependent phase delay for the shear body wave phases, *S*, and *SS*, and the minor arc surface waves, *R*, and *G* phases constrain the velocity and anisotropy structure in the layers. Phase delays are measured using the isolation filter technique on three-component seismograms. Observed phase delays show the large splitting of the *SH* and *SV* components, which indicates shallow polarization anisotropy. The combined dataset, 17 *ScS* reverberation data and more than 1000 frequency-dependent phase delays, was inverted for a path-averaged one-dimensional, radial anisotropic model. In order to obtain a geophysically and geologically acceptable mode *a priori* information such as mineralogical constraints of bulk sound velocity and density used below 250 km depth are incorporated in the inversion. The final model, named PHB3, is characterized by a 15 km thick crust, an anisotropic lid bounded by a sharp negative discontinuity at 89 km, a low-velocity zone with its anisotropy tapered off at 166 km, an isotropic of steep velocity gradient to 408 km, and transition zone discontinuities at 408 km, 520 km, and 664 km depth. The lid velocities and its thickness are significantly lower and thicker than those in a comparable model for the Pacific, respectively, and these differences, which cannot be explained solely by the temperature difference, likely reflect the compositional variation in the lithosphere of the two regions. We suggest that the thickness of the lithosphere is controlled by the melting depth at the stage of basalt depletion, and that a thick crust and a thick and slow lithosphere in the Philippine Sea are the consequence the higher water content in the upper mantle, possibly related to its origin in the back-arc.

Table of contents

Chapter 1: Introduction

One of the major contributions of seismology to the development of the plate tectonics theory has been the elucidation of oceanic plate structure. In order to understand how the oceanic plate grows and how the upper mantle evolves, it is essential to understand the shallow structure of the upper mantle. Knowledge of oceanic lithosphere and asthenosphere underlying it, including the relation between surface tectonics and deep structure, serves as basic data for the study of chemical, mineralogical and dynamic processes of the oceanic upper mantle.

The oceanic upper mantle has been studied previously the analysis of surface waves, especially their group and phase velocity dispersion (see *Nakanishi* [1992] for a review). While the lack of seismographic stations in ocean basins limits the use of body waves, even a small number of observations of surface waves, which are sensitive to the shallow structure along the path, provides useful information of the upper mantle and, as a result, makes it possible to investigate the structure in oceanic region. In a long period record, surface waves of shallow events consist mostly of the fundamental mode branch, for which phase and group velocities are determined by the shallow upper mantle structure. In order to investigate deep structure, it is necessary to isolate the higher mode portion of surface waves and to measure their dispersion. For shallow events, the amplitudes of higher mode surface waves are usually smaller than those of fundamental modes, making it difficult to carry out an unbiased dispersion measurement. Even though intermediate events excite higher mode surface waves effectively so that their amplitude at the Earth's surface is relatively large, several wave groups arrive within a small time window, so that it is difficult to decompose complex waveform into branches for the measurement. A small number of previous successful studies took advantage of a certain geometry of source and station arrays and applied a methodology that requires heavy processing of array

seismograms [e.g. *Cara and Lévêque, 1987*], but these methods are difficult to apply in other regions.

The next phase of upper mantle models came with the advent of waveform inversion [*Woodhouse and Dziewonski*, 1984; *Tanimoto,* 1984] (see a recent review by *Li and Tanimoto* [1992]). Instead of viewing waveforms as a sum of phases or branches and trying separate phases and branches requiring separation, in this methodology the whole waveform is treated as data. With the help of waveform synthesis techniques, in theory we can reproduce any wavefield, however complex it should be, and can formulate an inverse problem for earth structure. This wholesale approach has apparently freed seismologists from the task of isolating and identifying phases and branches. However, because of such major problems as non-linearity between the structure and waveforms, as well as minor ones such as improper match due to cycle skipping, this technique is still in a developmental stage in global seismology, in which geometry of sampling is limited by the uneven distribution of earthquakes and seismic stations. Also it has become apparent that all the most modern global models resulting from waveform inversion do not reflect the strong lateral heterogeneity of the upper mantle structure, including characteristic difference between continental and oceanic upper mantle [*Gaherty and Jordan,* 1995; *Gaherty,* 1995]. Even among oceanic provinces, strong lateral variations of discontinuity depths and their reflectivities exist [*Revenaugh and Jordan,* 1991a-d], indicating the limitation of a one-size-fits-all approach. As a result, several intermediate techniques using waveforms and extracting data functional and inverting them have been proposed [*Nolet,* 1992; *Gee and Jordan*, 1992], and their applications have just started to bring in new interesting result [*e.g. Zielhaus and Nolet,* 1994; *Gaherty and Jordan*, 1995]. In particular, our knowledge on several key issues on the upper mantle structure such as depth extent of anisotropy and relation between age and lithosphere thickness is rapidly increasing.

In this thesis, we investigate the upper mantle structure beneath the seismic corridor in the Philippine Sea. The path traverses the western part of the Philippine Sea plate,

between the seismic zone in the Sumba and Philippine Islands and GSN station MAJO in central Japan (Fig. 1.1). A major part of the Philippine Sea plate originated by back-arc spreading, which is unique to this plate. West of Kyushu-Palau ridge is the Western Philippine basin (opened between 35 and 50 Ma), and on the other side of Kyushu-Palau ridge is Shikoku basin in the north, currently subducting northward beneath the Eurasian plate (opened 15-25 Ma), and Parece Vela basin (opened 18-32 Ma) in the south. Along the eastern edge of the plate spreading has been active for the last 5 Ma between West Mariana ridge and the Mariana basin [*Tamaki and Honza,* 1991] (Fig. 1.2). The sampled area in our study is the older half of this plate, the Western Philippine Sea Basin and Shikoku Basin, which are two major back-arc basins [*Taylor and Karner,* 1983]. The origin of the Western Philippine Basin has been in dispute, and *Ben-Avraham and Uyeda* [1983] argued that this basin is a normal oceanic basin trapped by its break-up. However, the recent geological and geophysical evidence favors the reconstruction in which the Western Philippine Sea basin was originated by back-arc spreading, with the Central Philippine Fault being the spreading center [*Hall et al.,* 1995].

One of interesting observations in the Philippine Sea basin is that its sea depth is abnormally deep relative to that in normal ocean basins. While the age-depth relation in major oceans is well approximated as

$$Depth = 2{,}500 + 350\times\sqrt{Age}$$

[*Parsons and Sclater,* 1977], *Park et al.*, [1990] showed that age-depth data in the Philippine Sea is better fit by

$$Depth = 3{,}222 + 366\times\sqrt{Age},$$

which gives almost 1,000 m deeper sea depth for a sea-floor of the same age. *Park et al.* [1990] argued that since both relations give similar cooling curves the cooling process of plates should be similar in both environment , and hinted that the reason of this difference should be related to the material properties of the lithosphere. Recent re-evaluation of *Parson and Sclater* [1977]'s relation has given most attention to the Pacific [*e.g. McNutt,*

1995], which is the oldest oceanic plate and therefore abundant of data has been collected, and these new models [*Stein and Stein,* 1992; *Carlson and Johnson,* 1994] generally agree well with *Parson and Sclater* [1977]. There seems no strong evidence that distinguishes the Pacific from Philippine Sea other than their origins, and this depth difference has not yet been explained.

Another interesting observation in this corridor came from the *ScS* reverberation study by *Revenaugh and Jordan* [1991a-c]. Analyzing a family of *ScS* phases and energy reflected from internal discontinuities between Mohorovičić (M) discontinuity and core-mantle boundary (CMB) using stack and migration method, they revealed the existence of an unusually thick oceanic lithosphere in this corridor underlying a thick oceanic crust; beneath 15 km thick crust, they located a negative impedance contrast, the Gutenberg (G) discontinuity, at 85 km depth, indicating the high velocity lid in this region extends to a deeper depth than a conventional average oceanic mantle. This is significantly deeper than a comparable observation in the old oceanic basin in the Pacific; in a corridor between Hawaii and Tonga the G discontinuity was located at 59 km and the crustal thickness was a normal value of 6 km [*Revenaugh and Jordan* , 1991c]. Because a major part of the Western Philippine Sea basin had spread in current N-S direction, the sea floor age is less uniform than that along Hawaii-Tonga corridor. Nevertheless, confirmed magnetic anomalies in these basins span a fairly narrow range of 15-56 Ma [*Seno,* 1985; *Hall et al.,* 1995]. The relation between sea-floor age and lithospheric thickness (the depth from Moho to the G discontinuity) implies 30-50 km thick lithosphere in this age in the Pacific [*Regan and Anderson,* 1984; *Nishimura and Forsyth,* 1989], and the reason we have a thicker lithosphere in the young Philippine Sea is uncertain. *Revenaugh and Jordan* [1991c] observed a vertical travel time to a discontinuity, which is the product of layer thickness and slowness (inverse of velocity), and could not constrain either of these by itself, and we need additional observations on either lid thickness or *S* velocity, or both, to model the velocity structure better.

Our goal in this thesis is to present a radial anisotropic upper mantle model for the western Philippine Sea region. The recent advent of two completely different but complementary methods provides us a means to explore the wide variety of the regional upper mantle structure. *ScS* reverberation analysis provides the framework of upper mantle layering, the location of the major discontinuities and their brightness. Measurement of frequency-dependent travel times of body and surface wave phases using a cross-correlation technique helps constrain the velocity gradients in the layers. Combining these two methods and results, we can construct an upper mantle model from a self-consistent analysis of three-component seismograms. This combined method has been successfully applied to the western Pacific [*Gaherty*, 1995; *Gaherty et al.*, 1996] where they confirmed unambiguously the existence of polarization anisotropy in the low velocity zone for the first time.

One of the two types of anisotropy is generally assumed in modeling the upper mantle. The first is azimuthal anisotropy, which has a fast axis in horizontal direction with hexagonal or orthorhombic symmetry, and second is radial anisotropy, with a (usually) slow axis in the vertical direction and invariant horizontal velocity (also termed as "transverse isotropy", or "polarization anisotropy"). While it is likely that mineralogy of the upper mantle, evidently dominated by olivine, results in the former type of anisotropy in a local scale, the latter one is useful for two reasons: 1) an azimuthal anisotropy provides apparent radial anisotropy in azimuthally averaged data, or in data constrained in one azimuth, and 2) the lateral symmetry provides an easy treatment of modeling. Our source-receiver geometry is a narrowly confined corridor so that we presume that the radial anisotropy is a good approximation, in the sense that it can be used to model the path-averaged (azimuthally variable) anisotropy [*Maupin*, 1985]. Throughout this thesis we use the notation of *Dziewonski and Anderson* [1981], in which 6 parameters describe the radial anisotropic model at a given depth: 5 velocities v_{SH}, v_{SV}, v_{PH}, v_{PV}, and η, as well as density ρ. v_{SH} is the velocity of a horizontally propagating, transversely polarized shear

wave; v_{SV} is the velocity of a horizontally propagating, vertically polarized shear wave or a vertically propagating shear wave; and v_{PH} and v_{PV} are the velocities of a horizontally and a vertically propagating compressional wave, respectively.

In Chapter 2 we will describe our observations, especially how we measured our frequency dependent phase delay data. The measurement was performed by the method of *Gee and Jordan* [1992], which enables us to measure phase-delays of the complex wave groups observed at regional distances.

We then inverted these observations and *ScS* reverberation observation together for a radially anisotropic structure under an average-path assumption, as will be presented in Chapter 3. We used the non-linear Gaussian-Baysian procedure of *Tarantola and Valette* [1982]. In addition to our observations, we also incorporated *a priori* knowledge of upper mantle structure and mineralogy. This reduces the model space we needed to explore and at the same time makes the final model physically meaningful. Because our seismological observations were mostly sensitive to *S*-velocity, the inclusion of *a priori* information is particularly useful to constrain *P*-velocity and density in the inversion.

Our preferred final model will be presented in Chapter 4, and its geophysical implications will be discussed in Chapter 5. Because of several past observations which showed the peculiar nature of the Philippine Sea plate, it is important to dissect this model in comparison to other models. We can also compare this model with another oceanic upper mantle model derived by a similar methodology, model PA5 for the old Pacific basin [*Gaherty*, 1995; *Gaherty, et al.*, 1996]. This comparison will help us understand the growth of oceanic plate and the evolution of the upper mantle.

FIGURE CAPTIONS

Fig. 1.1 Mercator projection of the Philippine Islands-to-Japan corridor studied in this study. Star denotes GSN station MAJO. Epicenters of the 28 Philippine Islands events used in phase delay measurement are also shown.

Fig. 1.2 Principle tectonic, bathymetric and magnetic features of the Philippine Sea region from *Hill et al.* [1995]. The propagation path from Philippine Islands to Japan crosses magnetic anomalies in the Western Philippine Basin, but the oldest part of the path is about 56 Ma.

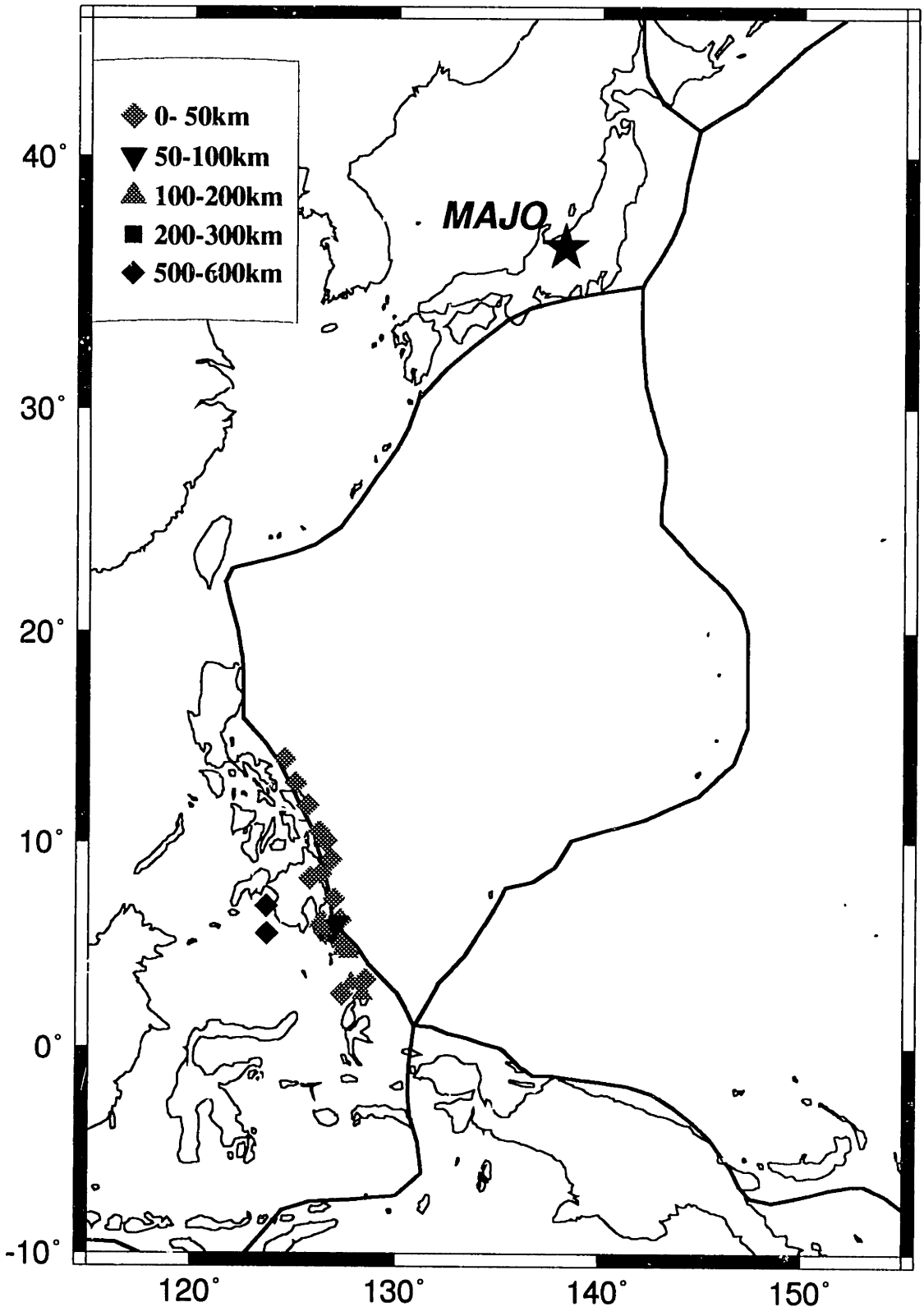
0- 50km
50-100km
100-200km
200-300km
500-600km
MAJO
40°
30°
20°
10°
0°
-10°
120°
130°
140°
150°

Figure 1.1

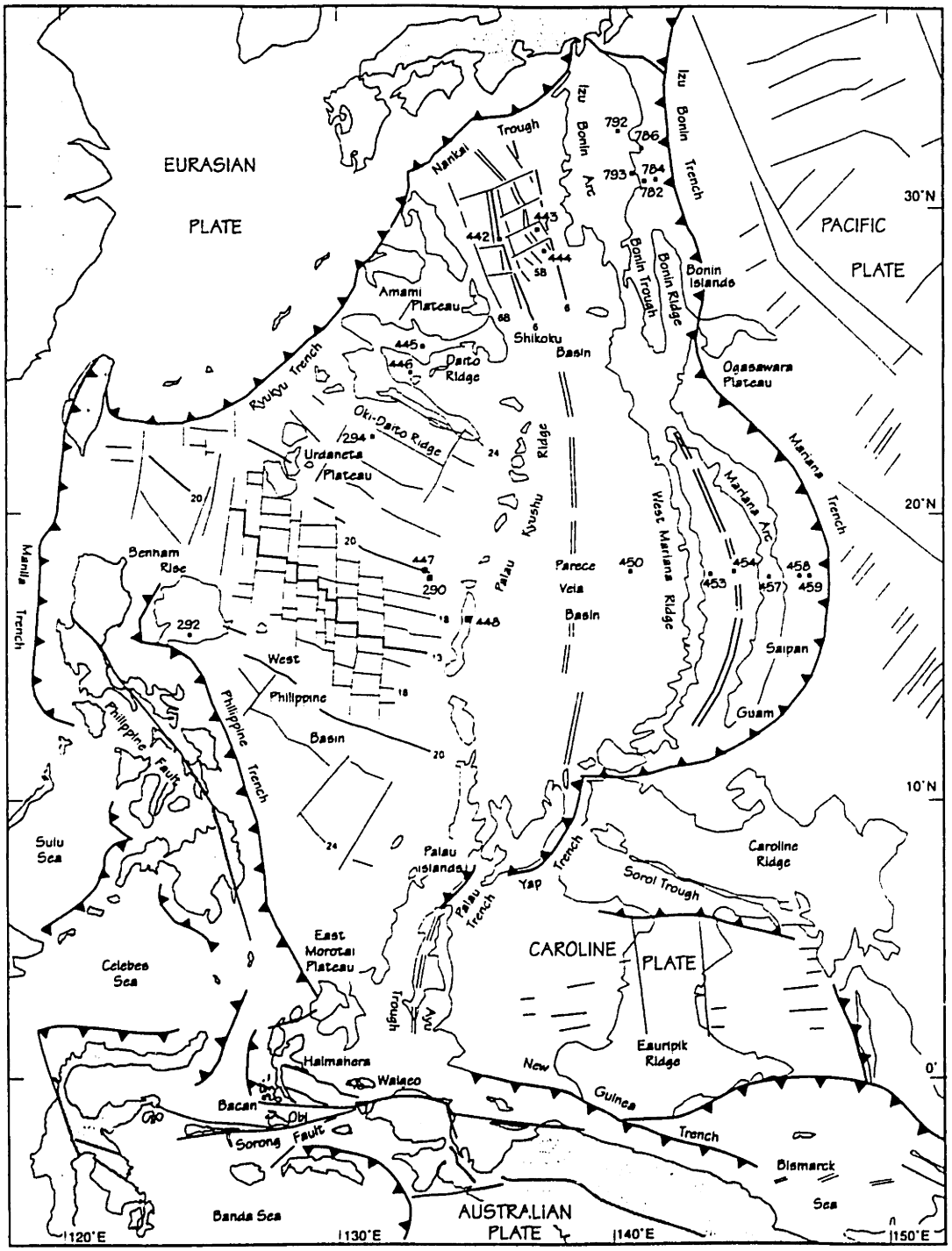
EURASIAN
PLATE
PACIFIC
PLATE
CAROLINE
PLATE
AUSTRALIAN
PLATE
Izu Bonin Trench
Izu Bonin Arc
Nankai Trough
Bonin Islands
Bonin Trough
Bonin Ridge
Ogasawara Plateau
Amami Plateau
Shikoku Basin
Daito Ridge
Ryukyu Trench
Oki-Daito Ridge
Urdaneta Plateau
Kyushu Ridge
Mariana Trench
Mariana Arc
West Mariana Ridge
Parece Vela Basin
Palau Ridge
Benham Rise
West Philippine Basin
Philippine Trench
Philippine Fault
Manila Trench
Saipan
Guam
Sulu Sea
Celebes Sea
Palau Islands
Palau Trench
Yap Trench
Sorol Trough
Caroline Ridge
East Morotai Plateau
Ayu Trough
Halmahera
Walaco
Bacan
Obi
Sorong Fault
New Guinea Trench
Eauripik Ridge
Bismarck Sea
Banda Sea
30°N
20°N
10°N
0°
120°E
130°E
140°E
150°E

Figure 1.2

Chapter 2: Data

To model upper mantle, two key components are important: depths to the discontinuities, and elastic parameters and the density in the layers. If we do not have sufficient data on either of them and have to use an assumption, the resultant model is only as good as that assumption. For example, *Regan and Anderson* [1984] started with a layered structure similar to PREM which has a large 220-km discontinuity and discussed the relation between age of lithosphere and its velocity structure. There is no firm evidence presented in their argument that supported their assumption and it is not straightforward to interpret their conclusion on the relation between sea-floor age and shallow structure. In another example, *Gaherty* [1995] showed that because of large the L discontinuity in their initial model PREM, the global S12-WM13 [*Su et al.*, 1995] model does not fit surface waveforms well for data low-pass filtered at 35 mHz. Therefore it is important to incorporate proper discontinuity structure in modeling upper mantle structure.

2.1 Reverberation data

In our methodology, the framework of layering, that is the depth to and impedance across the major discontinuities, was mainly constrained by *ScS* reverberation data, presented by *Revenaugh and Jordan* [1991a, c]. Specifically, we used vertical travel times (t_d) to and shear impedance contrasts (R_d) across discontinuities. Shear impedance at a given discontinuity at depth d is defined as

$$R_d = (\rho^- v_{sv}^- - \rho^+ v_{sv}^+)/(\rho^- v_{sv}^- + \rho^+ v_{sv}^+)$$

where ρ^- and v_{sv}^- are the density and *SV*-velocity just below d, respectively, and ρ^+ and v_{sv}^+ are the density and *SV*-velocity just above d, respectively. Note that in a radial anisotropic Earth model, the velocity of the vertically traveling *S*-wave is equal to *SV*-velocity [*Anderson*, 1989].

We used *ScS* reverberation data directly from *Revenaugh and Jordan* [1991a, Table 2; 1991c, Table A1], whose notation of discontinuities is used hereafter. For this corridor, their corridor #9, they found an H discontinuity (at 49 km, shear impedance contrast of 1.9%), a G discontinuity (86 km, -2.3%),and 410-km (412 km, 4.2%), 520-km (521 km, 0.8%), and 660-km discontinuities (660 km, 5.8%) (Fig. 2.1). Amplitudes of signal from the H and 520-km discontinuities were comparable to the noise level, but the addition of these two improved the match between data and synthetic reflectivity profiles and thus are included in the final reflectivity mode. Missing was the L discontinuity, which was observed on paths which sampled continental upper mantle [*Revenaugh and Jordan*, 1991c], and was interpreted as the termination of an anisotropic mechanical boundary layer [*Revenaugh and Jordan*, 1991c; *Gaherty and Jordan, 1995*]. These depths and impedance contrasts are derived by stack and migration method [*Revenaugh and Jordan*, 1989] and thus should represent averages along the path.

2.2 Phase delay observations

Velocity, its gradient, and anisotropy between discontinuities were constrained by frequency-dependent phase delay data of surface and body waves. We measured phase delays of 183 surface (*R1*, and *G1*), multiply-reflected (*sS, SS,* and *sSS)*, and direct (*S*) body waveforms from three-component, long-period digital seismograms of 28 earthquakes in Philippine Islands region recorded at GSN station MAJO in central Japan (Fig. 1.1). Seismograms were rotated into tangential-radial-vertical coordinate system and then were filtered between 5 and 45 mHz. The selected earthquakes were mostly of moderate sizes, with Mw ranging between 5.2 and 7.0, minimizing unmodeled source effects, and ranged in source depth from 14 km to 599 km and were at epicentral distances from 25 to 37 degrees (Table 2.1). Most of our events are in the northern half of the source region for path 9 in *Revenaugh and Jordan* [1991a-c].

We also measured phase delays from seismograms of 37 additional events, which are distributed over the entire source region for path 9 in *Revenaugh and Jordan* [1991a-c]. However, probably due to the lateral heterogeneous velocity structure in this region, observed waveforms were typically more complex than those in Tonga-Hawaii corridor [*Gaherty*, 1995], and it was difficult to make a large number of good measurements. This complexity limits the use of events with larger epicentral distances that would provide less complex multiply-reflected phases such as *SS*, *sSS*, and *SSS* phases which are useful in modeling structure in the lid and low-velocity zone [*Gaherty*, 1995; *Gaherty et al.*, 1996]. Figure 2.2 shows examples of waveforms from four events, two for the Philippine Sea path, two for the Pacific path. Events with similar depths and epicentral distances were selected for the comparison. Since radiation patterns of events were not similar an exact comparison is not possible, but still you can see differences in group velocity, especially of the *R* phase, and at the same time the complexity of Philippine Sea data, which is characterized by multiple arrival of surface wave phases possibly due to the lateral refraction.

GSDF Analysis

We analyzed these waveforms using the Generalized Seismological Data Functional (GSDF) methodology developed by *Gee and Jordan* [1992]. This analysis utilizes our ability to create accurate synthetic seismograms for a realistic Earth model. Upper mantle phases recorded in regional distances are often complex because of the interference of discontinuities, and several phases arrive in a short time interval. These phases are difficult to isolate in observed and synthetic three-component seismograms with conventional theories such as ray theory and normal-mode theory. Taking account of interference with other phases with close group velocity, GSDF makes the phase-delay measurement of complex phases possible [*Gee and Jordan*, 1992; *Gaherty*, 1995; *Gaherty et al.*, 1996].

This analysis consists of four steps; 1) creating an isolation filter, 2) cross-correlating with seismograms, 3) windowing and filtering of the cross-correlation functions, and 4) extracting four data functionals. Following the formalism of *Gee and Jordan* [1992], and its application by *Gaherty* [1995], we used normal mode summation to calculate synthetic seismograms, which are complete to 50 mHz, and included the effect of attenuation. We used the Harvard CMT catalogue [*Dziewonski et al.*, 1981] for source parameters.

Because of lack of good reference model for this region, we first constructed an initial isotropic model by forward modeling of waveforms using *ScS* reverberation data; beneath the crust, velocity and density jumps were introduced at each discontinuity to match observed shear impedance. Velocity gradients were held constant in the layers. We assumed an average sea depth of 5.4 km [*Mammerickx et al.*, 1978] and sediment thickness of 0.1 km [*Mrozowski and Hayes*, 1978; *Park et al.*, 1990]. The effect of sediment on waveforms was tested with alternative models with 5 km water and 0.5 km sediment in a couple of cases, but the differences in the surface wave waveforms were not significant by visual inspection. Though existence of reflector at the D" layer was found 305 km above CMB with impedance contrast of 2.2% [*Revenaugh and Jordan,* 1991d], our dataset is insufficient to resolve such deep structure in the lower mantle. The lower mantle beneath 771 km was fixed to PREM.

To explain the observed waveforms, we divided the region between the G and 410-km discontinuities into two layers with a boundary at about 160 km. L discontinuities around this depth, which is primarily a signature of the continent [e.g. *Revenaugh and Jordan,* 1991b], have been found in many regions, including the corridor between New Britain Islands and GSN station TATO in Taiwan (path #17, in which L discontinuity is at 227 km with impedance contrast of 1.1%), which crosses the southern half of our corridor. However, since this "L discontinuity" was not found in our particular corridor, during

forward modeling we treated this as second order discontinuity, where neither velocity nor density jumps are allowed.

Our initial model, PHB, shown in Figure 2.3, is an isotropic model throughout the upper mantle, and has a lid structure that is less significant than commonly assumed for an oceanic mantle. In this model, discontinuities are at 20.5 km (M), 50.2 km (H), 90.2 km (G), 156 km (L), 415 km (410-km), 523 km (520-km), and 674 km (660-km).

Comparison between data and synthetics from isotropic model synthetics shows that observed group velocities of Rayleigh waves were lower and those of Love waves were higher than the model prediction. For example, waveforms in Figure 2.4 show that relative to synthetic prediction from isotropic model, Love waves arrive earlier and simultaneously Rayleigh waves arrive later. This observation is one of the diagnostics of polarization anisotropy in the shallow mantle [*Gee and Jordan,* 1988; *Gaherty and Jordan,* 1995].

Attenuation structure of the upper mantle is not well understood but is necessary for calculating waveforms and isolation filters, and we assumed a simple structure with four layers. *Revenaugh and Jordan* [1991a] concluded from waveform inversion that the attenuation factor for whole mantle, Q_{ScS}, for this corridor is 181. We assumed that lower mantle was globally laterally homogenous and used the attenuation factor for lower mantle, Q_{LM}, of 231 [*Revenaugh and Jordan,* 1987] which was obtained for the corridor between Hawaii and Tonga region. This then gave the attenuation factor for the upper mantle, Q_{UM}, of 121. As we expected a significantly lower Q (stronger attenuation) in the low-velocity zone compared to in the lid and transition zone, we partitioned Q_{UM} into Q_{LID} =140, Q_{LVZ} = 55, Q_{TZ} = 140, which roughly gave the same average Q_{UM}. We tested this attenuation structure with uniform upper mantle model with Q_{UM} =121 and Q_{UM} =91, and other than a reduction in the amplitude of the entire waveform, there is no significant difference in waveforms.

We created isolation filters for *S*, *SS*, *G*, and *R* phases using weighted subsets of normal modes selected by their phase and group velocities and branches. Specifically, isolation filters for *R* and *G* phases were constructed with fundamental branch modes. For isolation filters for body wave phases, modes were selected according to the observed group arrival time of the particular phase. Some core-reflected phases have similar arrival times as *S* or *SS* phases, but they have much smaller horizontal slowness (larger phase velocities). A phase velocity cut-off was then used to eliminated these core-interaction modes. Lower velocities were used as the maximum for *SS* phase isolation filters, as *SS* phases have larger horizontal slowness than *S* phases. Because of the small difference of group arrival times, for example, *SS* isolations filter often contain substantial energy of *sS* phase, and the same thing happens with *S* and *sS* phases, but use of this notation allows us to group isolation filters according to the maximum of their sensitivity: *SS* phases samples shallower part of the upper mantle than *S* phases.

Figure 2.5 and 2.6 give a graphic example of GSDF process for a measurement of the phase delay of an *SS* phase, and of a surface wave, respectively. First, the isolation filter was cross-correlated with both observed and synthetic seismograms (Fig. 2.5a, 2.6a), resulting in two broad-band cross-correlograms. Resultant correlograms were windowed to localize them in the time domain, and then narrow-band filtered to localize the signals in the frequency domain. We typically used 8 equally spaced bands between 10 and 45 mHz. Four data functionals were extracted from the narrow-band correlograms. Those from the synthetic correlograms were used to correct interference in the data that could not be removed by windowing. We used only the phase-delay functional, or frequency dependent travel time (Fig. 2.5b, 2.6b). Phase-delay measurements are useful as data, since the first-order relation between these and the model parameters is easy to compute. See *Gee and Jordan* [1992] and *Gaherty et al.* [1995] for details.

During the measurement process, qualities of the isolation filter (how good the isolation was in the synthetic seismogram) and cross correlation (measure of how good the

isolation was in the observed waveforms) were examined. Typically we discarded measurements at high frequencies for *R* and *G* phases and at low frequencies of *S* and *SS* phases based on their frequency content in observed seismograms.

Total number of travel times is 1039 from 183 wave groups. Figure 2.7 shows the summary of phase delay in 5 mHz interval, observed residuals relative to the isotropic starting model PHB for the 28 events used in the final inversion. In this plot, measurements were grouped according to their components (*P-SV* vs. *SH*) and phases, and variations of residuals at different hypocentral depth and epicentral distance, clearly seen in raw data, are not properly represented here. This plot does, however, show an indication of the existence of polarization anisotropy in the upper mantle as generally observed ($v_{SH} > v_{SV}$).

Table 2.1 List of Events

Date			Origin Time UT	Latitude °N	Longitude °E	Depth km	Distance °
1982	01	24	06:09:03.7	14.07	124.53	19	25.508
1987	11	18	16:27:08.7	12.93	125.04	29	26.320
198	10	26	05:14:20.2	11.84	125.65	20	27.075
1987	06	06	18:40:33.4	10.56	126.19	16	28.060
1991	06	15	23:02:14.2	10.10	126.55	35	28.360
1991	02	18	02:37:35.1	9.15	126.79	28	29.180
1980	04	13	05:41:48.8	8.47	126.31	27	29.969
1983	08	27	18:49:51.5	8.27	125.78	14	30.334
1992	05	17	09:49:29.4	7.27	126.96	34	30.890
1983	07	20	22:57:16.9	6.27	127.28	17	31.748
1980	02	29	11:13:30.6	6.13	127.17	79	31.912
1980	01	02	20:58:48.6	6.14	126.41	38	32.130
1987	11	07	16:23:57.2	5.90	127.04	73	32.169
1979	02	11	22:22:24.9	6.13	126.24	143	32.193
1977	11	21	11:39:46.4	6.92	123.64	599	32.351
1980	01	03	20:22:30.5	5.81	126.41	107	32.442
1980	01	08	10:08:49.0	5.73	126.29	100	32.554
1986	06	17	10:38:22.1	5.47	126.91	65	32.615
1983	07	14	19:47:50.2	5.57	126.58	33	32.618
1979	02	07	21:02:09.5	5.13	127.29	129	32.830
1987	10	29	20:23:44.9	4.78	127.67	142	33.060
1985	06	04	03:56:29.1	4.79	127.38	117	33.129
1987	05	11	09:59:37.7	4.65	127.65	116	33.190
1979	04	15	22:14:57.3	5.56	123.66	536	33.598
1991	07	21	22:59:15.1	3.33	128.51	40	34.561
1986	10	04	02:00:12.3	3.09	127.79	128	34.648
1983	05	11	00:17:16.9	2.61	128.35	133	34.971
1986	08	17	15:27:51.7	2.59	127.35	25	35.242

Harvard CMT Location

FIGURE CAPTIONS

Fig. 2.1 Observed reflectivity profile and its interpretation obtained for the Philippine Sea corridor (Left) and the Pacific corridor (Right) [*Revenaugh and Jordan*, 1991c]. The profile and its interpretation both display vertical shear impedance in percent. Apparent depths in interpretation were computed using PREM, and model M84C [*Woodhouse and Dziewonski*, 1984].

Fig. 2.2 Direct comparison of data complexity along the Philippine Sea and Pacific paths. First four traces are example of data of shallow events: top pairs of traces are transverse component data in the Philippine Sea path (top) and in the Pacific path (bottom), and the next two are vertical components. Next four traces are example of data of intermediate events: top pairs of traces are transverse component data in the Philippine Sea path (top) and in the Pacific path (bottom), and the next two are vertical components. The traces are aligned at 0 min on the *S* phase, and are band-passed between 5 and 45 mHz. In each pair data from the Philippine Sea path are more complex than that from the Pacific path, while in general surface waves have lower group velocities in the former than in the latter.

Fig. 2.3 Initial model PHB. From left to right, η, density, shear velocity, and compressional velocity are plotted as a function of depth. The model is isotropic through the upper mantle. Below 771 km depth, PHB is identical to PREM.

Fig. 2.4 Direct observational evidence of anisotropy in long-period seismograms. Transverse and vertical component waveforms from two events are shown along with the synthetic seismograms for PHB. The traces are aligned at 0 min on the *S* phase, and are band-passed between 5 and 50 mHz. Top four traces are of shallow (19 km depth) event. While group arrival of the Love wave in data is slightly earlier than that in the PHB

synthetic, group arrival of the Rayleigh wave in data is slightly later than that in the PHB synthetic. Similar pattern of group arrivals is also seen for another slightly deeper event (78 km depth).

Fig. 2.5 Example of the GSDF processing, as discussed in the text. a) Observed (top), full synthetic (initial model PHB, middle), and isolation filter (bottom) seismograms for transverse-component data from a deep focus event (599 km depth). The isolation filter is for *SS* phase constructed by summing normal modes with group velocities of 4.40 ± 0.3 km/s excluding fundamental mode. b) Phase delays $\delta\tau_p$ as a function of frequency, relative to the starting model. The frequency-dependent trend indicates the relative dispersion observed in these "body" waves, and illustrates the value of using a broad-band approach to processing the data. c) Three sets of partial derivative kernels as a function of depth; the kernels relative to the two shear velocities for 20, 35, and 45 mHz are shown for this example. Solid line is the v_{SV} kernel, and dashed is for v_{SH}. While the low-frequency observation (20 mHz) is sensitive to average v_{SH} between 300 and 900 km, the higher-frequency observation (45 mHz) is sensitive to the transition zone velocities, especially near the discontinuities. Note that v_{SV} kernel is non-zero in the shallow upper mantle.

Fig. 2.6 Example of the GSDF processing for vertical-component *R* phase from an intermediate focus event (129 km depth), similar to that of Fig. 2.5.

Fig. 2.7 Summary of frequency-dependent travel time data. Phase delays are grouped by phase type (Surface wave, *SS*, or *S*), and then separated into tangential (*SH*) or radial and vertical (*SV*) observations, and averaged in 8 frequency bands. Symbols represent the residuals relative to PHB. Dispersion is indicated by a frequency-dependent trend, and evidence of anisotropy can be seen as a separation of the *SH* and *SV* observations for a

given phase type. a) Love and Rayleigh waves. b) *SS* waves. c) *S* waves. Error bars shows a weighted average of estimated *a priori* errors.

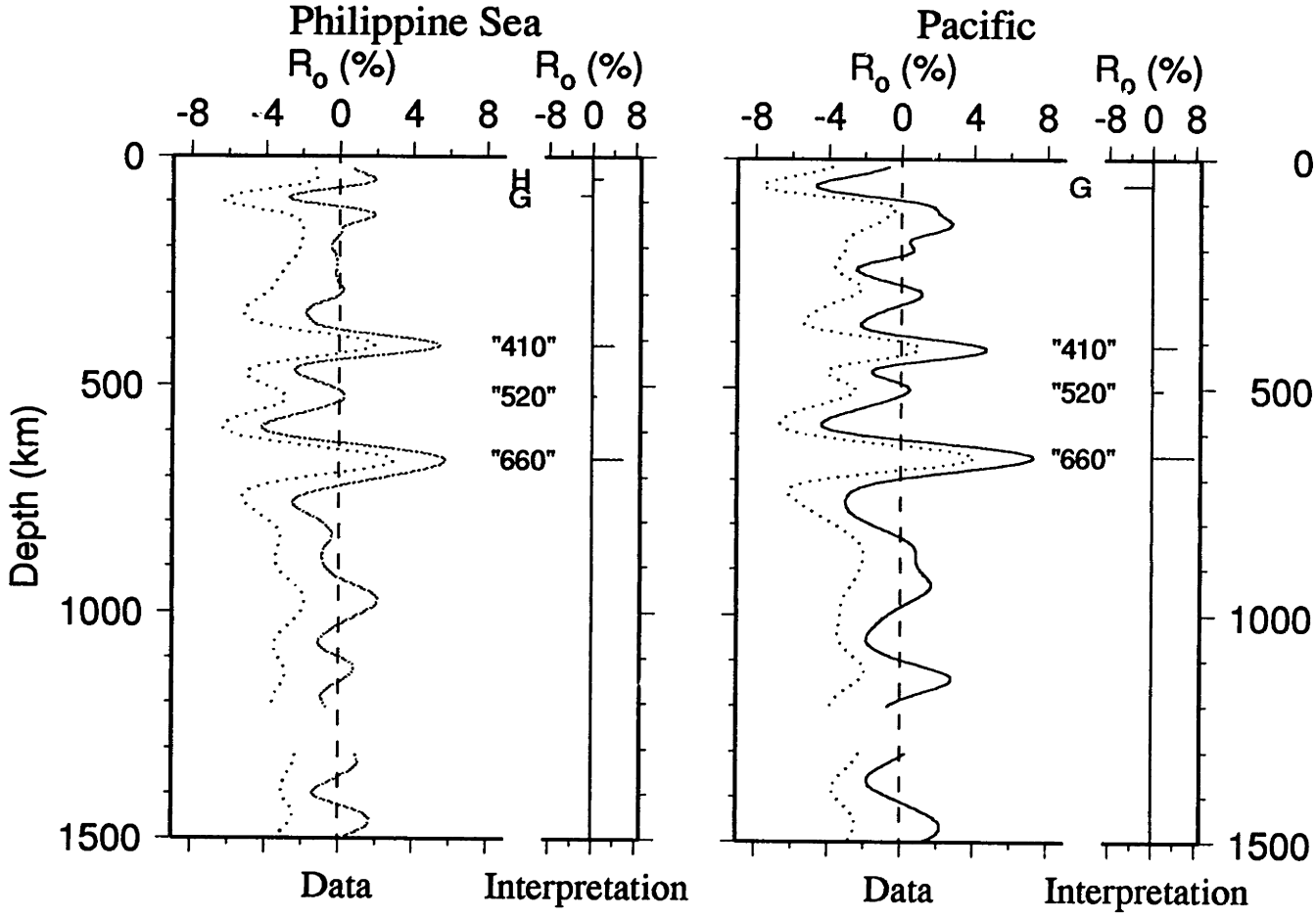

Revenaugh and Jordan, *J. Geophys. Res. 96,* 19781-19810, 1991

Figure 2.1

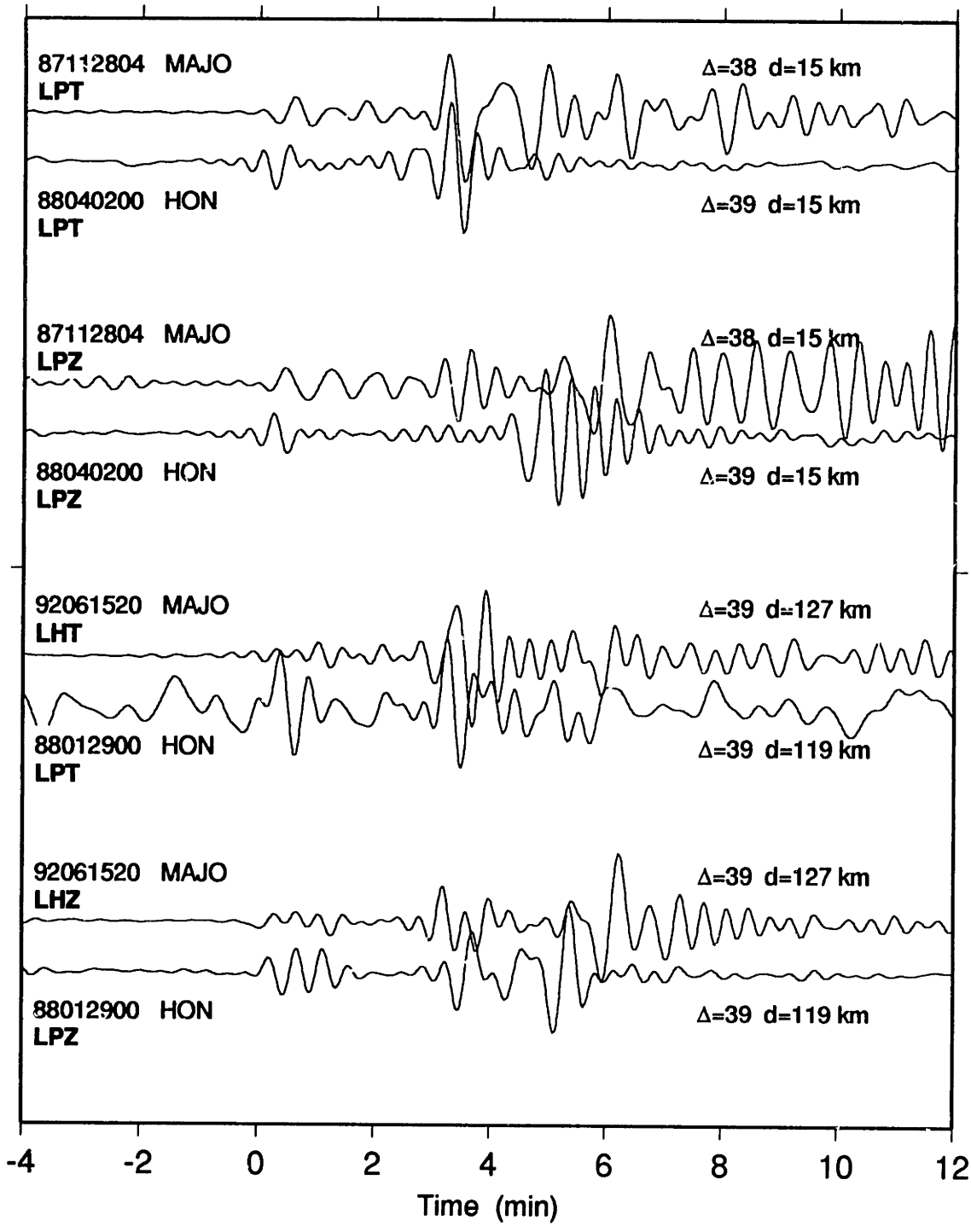
87112804 MAJO
LPT
Δ=38 d=15 km
88040200 HON
LPT
Δ=39 d=15 km
87112804 MAJO
LPZ
Δ=38 d=15 km
88040200 HON
LPZ
Δ=39 d=15 km
92061520 MAJO
LHT
Δ=39 d=127 km
88012900 HON
LPT
Δ=39 d=119 km
92061520 MAJO
LHZ
Δ=39 d=127 km
88012900 HON
LPZ
Δ=39 d=119 km
-4
-2
0
2
4
6
8
10
12
Time (min)

Figure 2.2

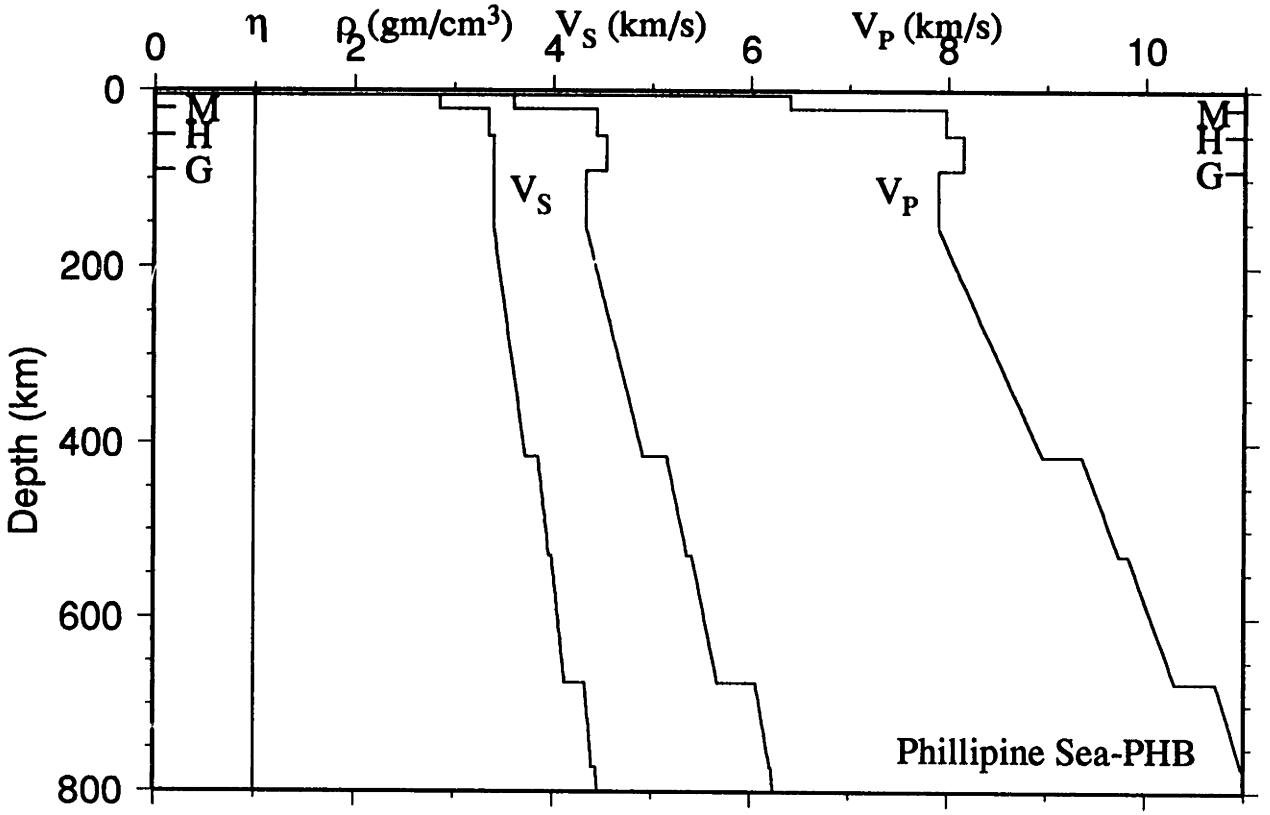
η
ρ (gm/cm³)
V_S (km/s)
V_P (km/s)
0
2
4
6
8
10
0
200
400
600
800
Depth (km)
M
H
G
V_S
V_P
M
H
G
Phillipine Sea-PHB

Figure 2.3

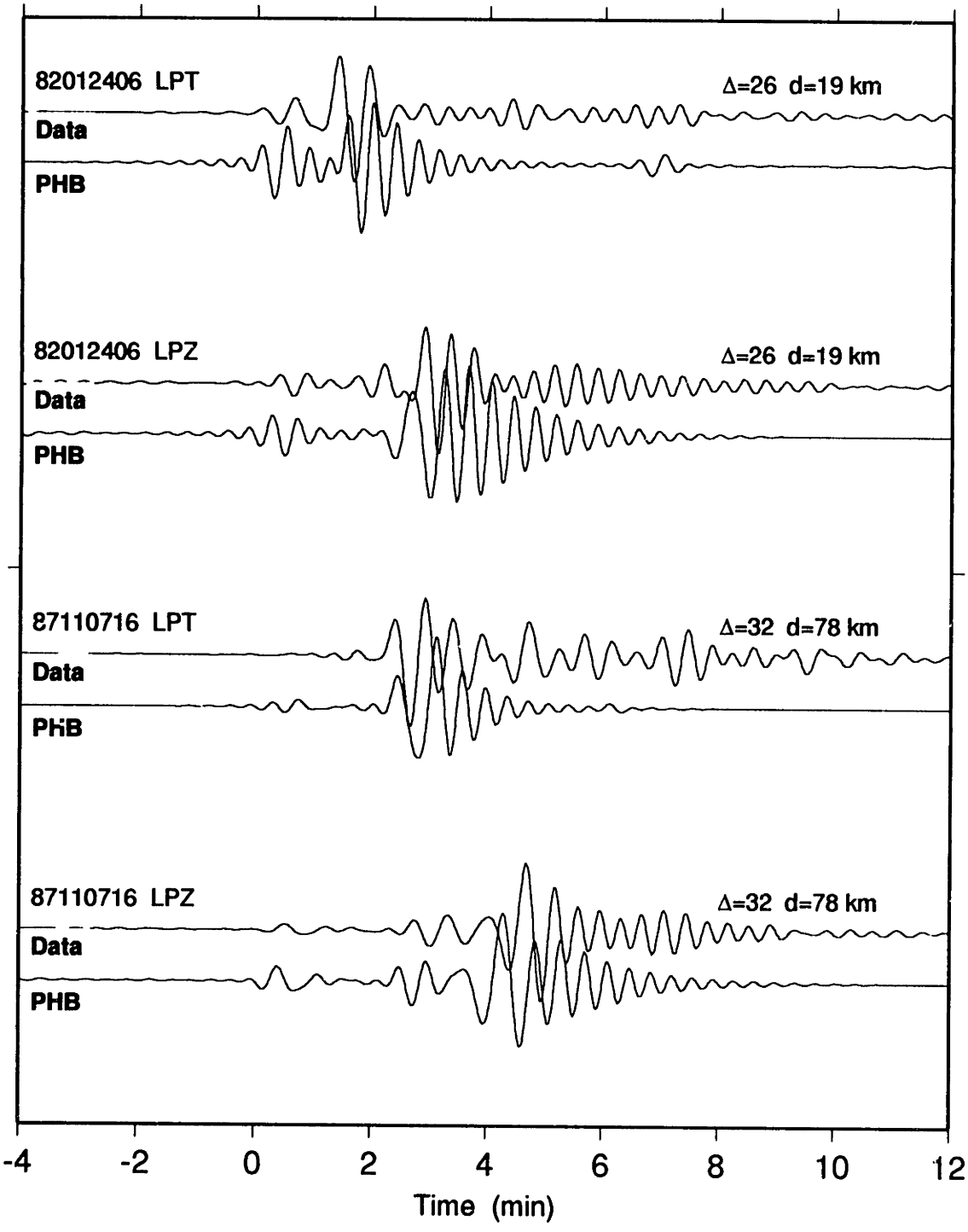
82012406 LPT
Δ=26 d=19 km
Data
PHB
82012406 LPZ
Δ=26 d=19 km
Data
PHB
87110716 LPT
Δ=32 d=78 km
Data
PHB
87110716 LPZ
Δ=32 d=78 km
Data
PHB
-4
-2
0
2
4
6
8
10
12
Time (min)

Figure 2.4

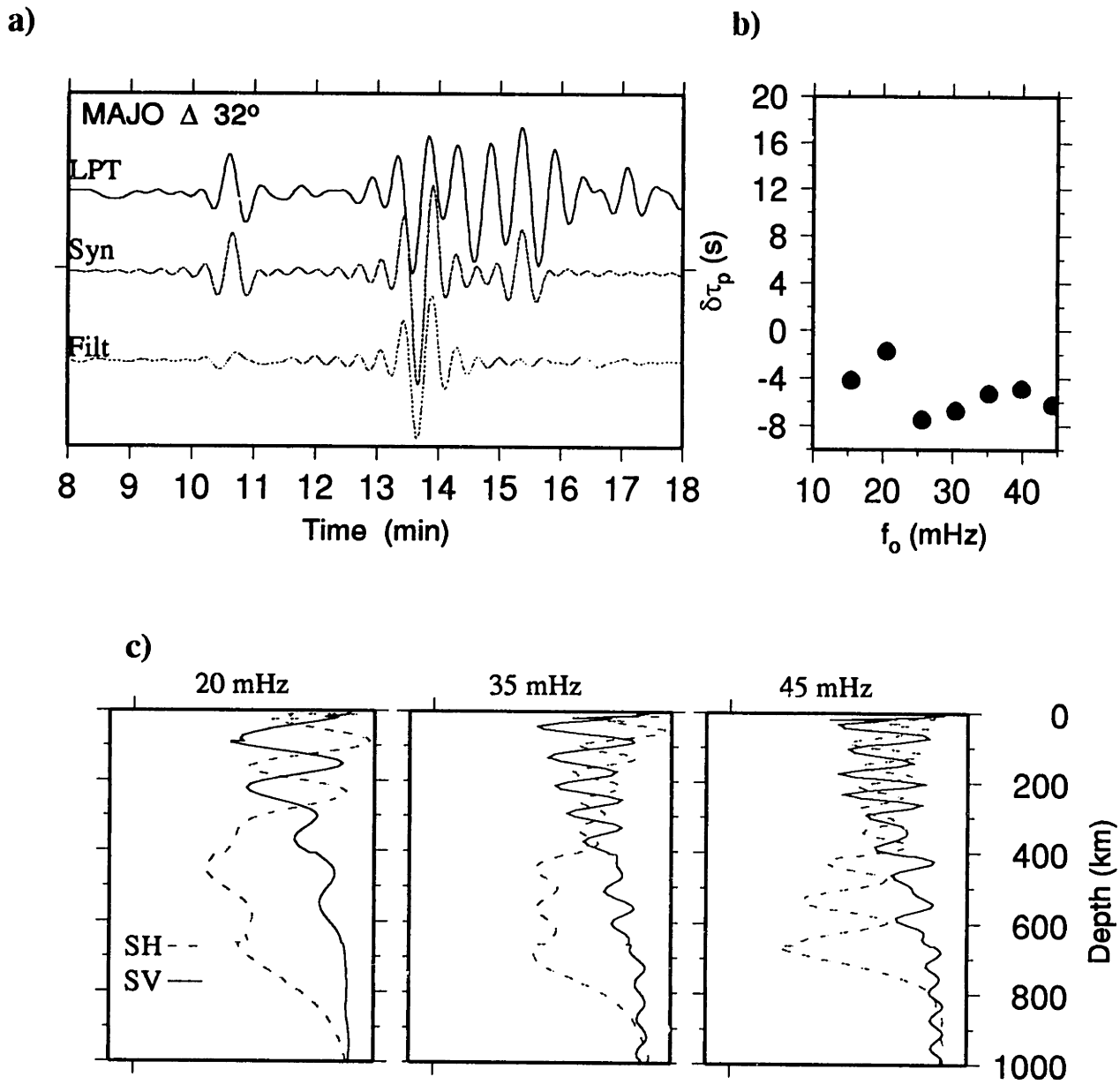
a)
b)
MAJO Δ 32°
LPT
Syn
Filt
8 9 10 11 12 13 14 15 16 17 18
Time (min)
δτp (s)
20
16
12
8
4
0
-4
-8
10 20 30 40
fo (mHz)
c)
20 mHz
35 mHz
45 mHz
SH - -
SV —
0
200
400
600
800
1000
Depth (km)

Figure 2.5

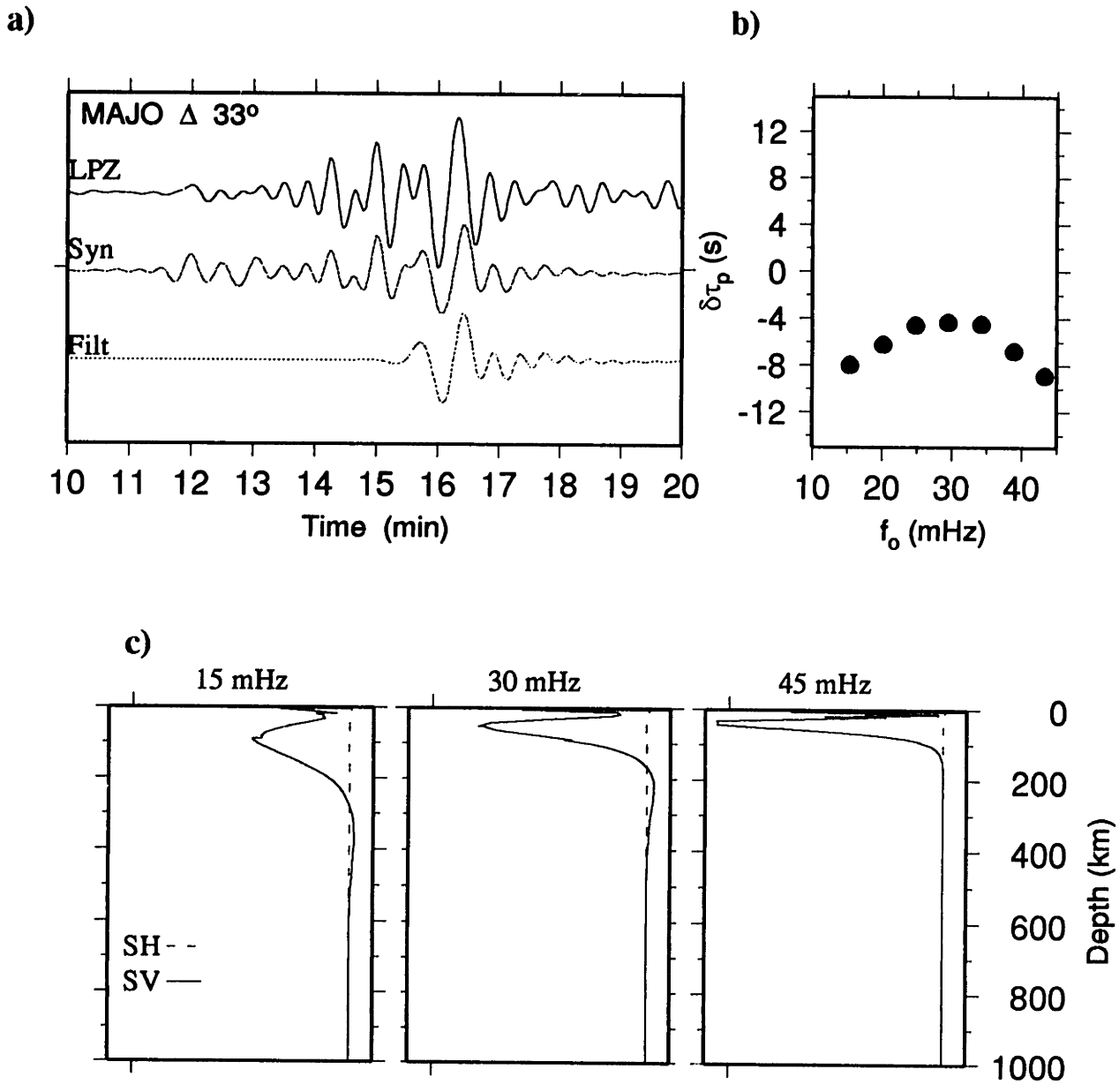
a)
b)
MAJO Δ 33°
LPZ
Syn
Filt
10 11 12 13 14 15 16 17 18 19 20
Time (min)
δτp (s)
12
8
4
0
-4
-8
-12
10 20 30 40
fo (mHz)
c)
15 mHz
30 mHz
45 mHz
SH - -
SV —
0
200
400
600
800
1000
Depth (km)

Figure 2.6

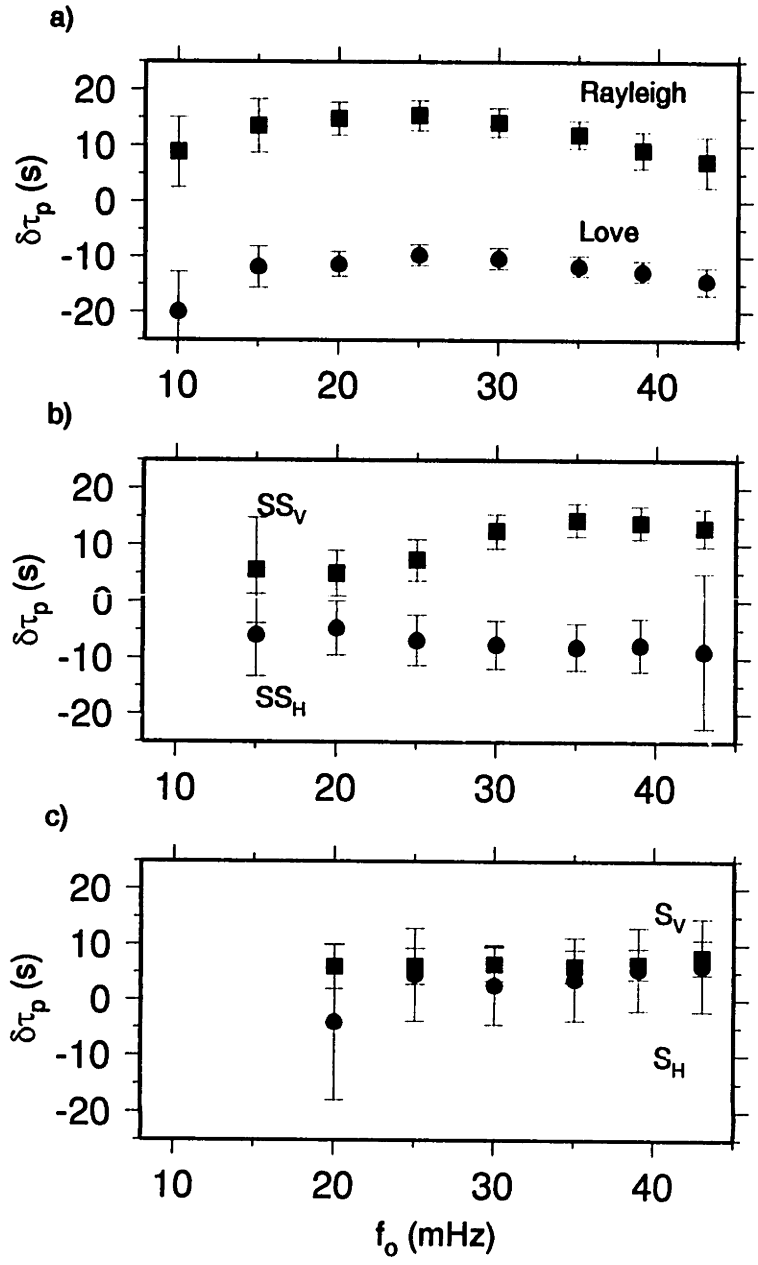
a)
Rayleigh
Love
b)
SS$_V$
SS$_H$
c)
S$_V$
S$_H$
$\delta\tau_p$ (s)
20
10
0
-10
-20
10
20
30
40
f$_o$ (mHz)

Figure 2.7

Chapter 3: Inversion

Inversion was started with the isotropic model PHB, derived from *ScS* reverberation data and forward modeling of waveforms (Figure 2.3). Model PHB was parameterized as a stack of layers, or spherical shells, bounded by sharp discontinuities. Each of 8 layers between crust to 771 km has 6 parameters, the five elastic parameters, v_{SH}, v_{SV}, v_{PH}, v_{PV}, and η as well as the density ρ, where we use the notation of *Dziewonski and Anderson* [1981], and constant gradients were assumed for all parameters in each layer. Throughout the inversion this basic framework was retained, while the location of discontinuity, velocities, and gradients within each layer were allowed to vary. The Q in each layer was fixed at the value given by the initial four-layer structure, and was assumed to be frequency-independent. We used the reference frequency of 35 mHz for the elastic parameters, and accounted for the physical dispersion due to the attenuation. Number of total model parameter was 110, which was a sum of 8 for discontinuity depth, 9 intercepts and 8 gradients for each of 5 velocities and density.

Inversion was carried out through two iterations. In kth iteration, the difference between the true model $\mathbf{m}$ and the current model estimate $\mathbf{m}_{k-1}$ was assumed to satisfy the linearized system

$$\mathbf{A}_{k-1}\,\delta\mathbf{m} + \mathbf{n} = \delta\mathbf{d}_{k-1},$$

where $\delta\mathbf{d}_{k-1}$ is the data-residual vector (difference between observation and prediction from $\mathbf{m}_{k-1}$), $\mathbf{A}_{k-1}$ is the partial derivative matrix computed from $\mathbf{m}_{k-1}$, and $\mathbf{n}$ is the data error. For *ScS* reverberation data, 8 reflection coefficients and 9 vertical travel times, the partials were calculated using ray theory and plane-wave reflection coefficients. To calculate the partials for frequency-dependent travel time observations, we used GSDF theory. Since we used modal summation to calculate isolation filters using a weighted subset of modes, we applied the same selections for the Fréchet kernels of normal mode eigenfunctions

computed for the current model estimate $\mathbf{m}_{k-1}$ to obtain the partial derivatives of the data with respect to the intercepts and slopes of model parameters and discontinuity depths. Examples of partial derivative are shown in Figure 2.5c and 2.6c.

The data-error $\mathbf{n}$ was assumed to have zero mean, with a diagonal covariance matrix $\mathbf{C}_{nn} = \langle \mathbf{n}\mathbf{n}^{\mathrm{T}} \rangle = \mathrm{diag}[\sigma_1^2, \sigma_2^2, \ldots, \sigma_N^2]$. For *ScS* reverberation data, the standard deviations (observational error estimates) σ_{R_d} and σ_{t_d} ranged from 0.005 to 0.010, and 1 to 2 s, respectively, which are given based on sharpness of discontinuities, and match of synthetic and observed reflectivity profile in *Revenaugh and Jordan* [1991c]. For the frequency-dependent phase delay data, standard deviations ranged from 2 to 20 seconds in the final iterate, which we assigned based on the quality of the observation and the expected resolution.

We used relatively low frequency waveforms, so that our use of CMT solutions [*Dziewonski et al.*, 1981] likely minimized any error associated with source parameters. To further minimize these errors, we defined raw source correction terms as weighted averaged measurements for *S* phase in 30 and 35 mHz bands, where measurements were mostly stable, for each event. Then the average of all source correction terms was used as the receiver correction term, and subsequently we subtracted this receiver term from each of the source correction terms. We then subtract resultant source correction terms from all phase delay measurements for that event. This use of *S* phase delay in eliminating source correction term is also useful to eliminate the effect of the lower mantle structure. Among our phases, *S* is the most sensitive to lower mantle structure, and this correction should minimize the projection of any phase delays caused by the difference between real and assumed lower mantle structure onto the upper mantle.

Gaussian-Bayesian Estimation

The perturbation $\delta\mathbf{m}$ was estimated by the nonlinear Gaussian-Bayesian procedure of *Tarantola and Valette* [1982]. We imposed an *a priori* Gaussian probability distribution

on $\delta\mathbf{m}$ having an expectation vector $\langle\delta\mathbf{m}\rangle = \overline{\mathbf{m}} - \mathbf{m}_{k-1}$ and a positive-definite covariance matrix $\langle\delta\mathbf{m}\,\delta\mathbf{m}^T\rangle = \mathbf{C}_{mm}$, and we calculated the estimate

$$\delta\mathbf{m}_k = [\mathbf{A}_{k-1}^T \mathbf{C}_{nn}^{-1} \mathbf{A}_{k-1} + \mathbf{C}_{mm}^{-1}]^{-1} [\mathbf{A}_{k-1}^T \mathbf{C}_{nn}^{-1} \delta\mathbf{d}_{k-1} + \mathbf{C}_{mm}^{-1}(\overline{\mathbf{m}} - \mathbf{m}_{k-1})].$$

After each step, the model was evaluated by a complete re-measurement of the data using synthetic seismograms and isolation filters computed for the new model $\mathbf{m}_k = \mathbf{m}_{k-1} + \delta\mathbf{m}_k$.

Our prior knowledge of earth structure is specified by the M-vector $\overline{\mathbf{m}}$ and the symmetric $M \times M$ matrix $\mathbf{C}_{mm}$. Several different types of information and assumptions were combined in their construction. Since our phase-delay data are less sensitive to P-velocity and density structure, we used density and bulk sound velocity ($\nu_\phi^2 = \nu_P^2 - \frac{4}{3}\nu_S^2$) profile for a pyrolite mineralogy by *Ita and Stixrude* [1992] as additional information [*Gaherty et al.*, 1996]. Their prediction based on laboratory data fits well with several upper mantle models, and they concluded these models were well explained by pyrolite model, and that models from different regions were equally well explained by a single pyrolite mineralogy model within the range of errors justifies the use of same mineralogical data for this corridor. Although their profile starts at 180 km depth, in their calculation the effect of the thermal boundary layer is not considered and at the same time it might not be appropriate to apply a standard compositional model to this shallow depth, where the lateral heterogeneity is expected to be strong, and we applied this between 250 and 750 km with standard deviation of 1%. Below 660-km discontinuity this constraint was lessened (± 3%) to allow both velocities and density to converge to PREM at 771 km discontinuity. While *Ita and Stixrude* [1992] concluded that pyrolite better matches the observed density and bulk sound velocity, their predicted values are similar for piclogitic models, and choice of composition does not critically change our result. In the low-velocity zone and above where we did not use mineralogical constraints, the ratio between average P and S velocities were weakly constrained to that of the initial model (within ± 10%).

Although we formulated our inversion to allow all layers to be anisotropic, limitation of our resolving power makes this unrealistic and data did not require this. Our formulation enables us to include isotropic layers by selectively forcing it ($v_{SH} = v_{SV}$, $v_{PH} = v_{PV}$, $\eta=1$) at the top and/or bottom of individual layer. By examining the misfit and trade-off, we examine each model to test the required depth extent of anisotropy. Specifically, in first iteration, our intermediate model PHB2 is anisotropic only between Moho and G discontinuity, while as we will show in the next chapter our final model is anisotropic down to L discontinuity. In addition, we constrained in anisotropic layers to be close η to the value in PREM ($\pm$ 5%); this value is also consistent with mineralogical calculations [*Nataf et al,* 1986].

Chapter 4: Results

Because our phase-delay measurements were relative to a reference model, it is necessary to repeat the entire measurements in each iterate. Iteration is essential, as there exists a strong non-linearity between the *S*-velocity of the lid and the low-velocity zone and phase and amplitude of SS and *G* phases. As we described in previous chapters, we started with isotropic PHB model. Updated model PHB2, radially anisotropic between the Moho and the G discontinuity, represents the second generation model. Using PHB2 as the initial model we reprocessed all GSDF data and inverted for a final model.

4.1 Model PHB3

Figure 4.1 shows model PHB3, our preferred and final model. A number of models could satisfy reverberation and phase delay data equally well, and also could explain observed waveforms. The waveform match between data and a model synthetic was hard to define quantitatively, especially with the presence of lateral heterogeneity, and selection of this model among many candidates was therefore subjective. However as far as we tested, the major characteristics in model PHB3 are robust.

PHB3 is radially anisotropic between the M and the L discontinuity, which is 166 km deep, and is characterized by a thick, low-velocity lid. Beneath the Moho at 17 km, the H discontinuity is at 51 km, and the G discontinuity is at 89 km, which means lid thickness is about 72 km. v_{SH} and v_{SV} in the lid are 4.54, and 4.39 km/s, respectively, between the M and H discontinuity, and 4.59 and 4.41 km/s, respectively, between the G and the L discontinuity. This thick slow lid was expected from large vertical travel time between M and G discontinuity found by *Revenaugh and Jordan* [1991c] (larger than in Tonga-to-Hawaii corridor); since vertical travel time was equal to total lid thickness divided by average *SV* velocity, lid with a typical *S*-velocity (e.g. 4.6125 km/s [*Dorman et al.*, 1960])

would be destined to be much thicker than a typical 50 Ma lid (30-50 km), and lid with a normal thickness needs extremely slow *SV* velocity to satisfy observed vertical travel time. We performed a series of experiments, both forward and inverse, but we could not find an acceptable model with either a typical *SV* velocity (with a thicker lid) or a typical lid thickness (with a much slower *SV* velocity).

Corresponding *P*-velocities are also low (v_{PH} and v_{PV} in lid are 8.02 and 7.91 km/s, respectively, between Moho and H discontinuity, and 8.14 and 8.00 km/s, respectively, between G and L discontinuity). However, this low *P*-velocity is consistent with the marine seismological observation by *Shimamura et al.* [1975]. *Shimamura et al.* [1975] analyzed apparent velocities of teleseismic *P* and *S* phases recorded their ocean bottom seismogram placed in the Western Philippine basin, and concluded that upper mantle velocity beneath the Philippine Sea was considerably lower than that in the Pacific basins (apparent v_P and v_S are 7.9 and 4.6 km/s, respectively, when the epicentral distance is ~12°; apparent v_P is 8.2-8.3 km/s in the Pacific). Also our model was in agreement with the observation of *Louden* [1980], who found apparent compressional velocity of 8.10±0.30 km/s in the Western Philippine basin from refraction experiments.

Anisotropy is terminated at the L discontinuity. *S* anisotropy in the lid is about 3.5 percent (3.4% between Moho and H, and 3.9 % between H and G), while *P* anisotropy is about 1.5 percent (1.4% between Moho and H, and 1.8 % between H and G). Both *S* and *P* anisotropy are the strongest just below G (*S* 4.9%, *P* 1.9%) and are tapered off at L discontinuity.

In the transition zone, 660-km discontinuity is at 664 km depth, which is slightly deeper than the observed global average of about 660 km [*Shearer and Masters,* 1993], and at the same time 410-km discontinuity is at 408 km depth, slightly shallower than their global average, 410 km [*Shearer and Masters,* 1993]. Although no deep (>700 km) discontinuity in this corridor was found in *ScS* reverberation study [*Revenaugh and Jordan,* 1991c], PHB3 has a small positive discontinuity at 761 km. We extrapolated

PREM upwardly to this discontinuity from 771-km discontinuity, below which PHB3 is identical to PREM [*Dziewonski and Anderson,* 1981]. It was technically possible to eliminate any jump in parameters at this depth, but since we did not perturb any structure in the lower mantle and none of our data had strong control over this depth range, we did not force this to be a second-order discontinuity.

Predicted vertical travel times and reflectivities for model PHB3 fit the observations quite well (Fig. 4.2). We found during several forward modeling experiments of waveforms that Moho reflectivity of *Revenaugh and Jordan* [1991a] did not necessary gives a good waveform match when a reasonable crustal velocity and a lid density are assumed, and did not try to force the final model to have crust structure which gave values close to their observation. As for GSDF data, PHB3 generally explains the phase delays reasonably well with an exception of *G* phase. Figure 4.3 summarized fit to the observed phase delay data, which shows the observed residuals and the predicted one. Part of misfit of *G* and *SS* phases could be attributed to the complexity of transverse component waveform. We speculate that because of the interaction with layered structure as well as a small scale heterogeneous anisotropic structure, several wave groups arrive in a short time interval, some of which could not be excited as a coupled mode between toroidal and spheroidal modes and could not be predicted by a one-dimensional model.

Figure 4.4 shows all observed waveforms and synthetics for PHB3. There are some obvious misfits between observed data and full synthetic waveform for model PHB3, both filtered between 5 and 45 mHz, match between them are fairly good. We found some difficulty modeling waveforms of intermediate events which samples the lid and low-velocity zone.

4.2 Comparison with previous models

It is ideal to compare this model against previous models obtained independently from different data and by other methods. A number of reports have been published since

Kanamori and Abe [1968]'s pioneering work on analysis of surface wave group velocity in this oceanic region. Most analyses used surface wave group velocity dispersion as their observation and the modelings are done with several assumptions.

Kanamori and Abe [1968] proposed a shear velocity model ARC-1 from three observations of group velocity dispersion, which has 5 km lid overlying 50 km low velocity zone (G discontinuity is at 30 km) (Fig. 4.5). As they noted there was a strong trade-off between lid velocity and its thickness, and they fixed lid velocity to 4.6125 km (model 8099 [*Dorman et al.* 1960]) and concluded that this region has a typical oceanic plate, which is characterized by a thin, high velocity lid. This model has been used as a reference model in a number of subsequent group velocity dispersion studies either implicitly or explicitly [*Seekins and Teng,* 1977; *Shiono et al.,* 1980; *Oda and Senna,* 1994]. Although *Oda and Senna* [1994] reported that average group velocity in the entire Philippine Sea plate, including active spreading along Mariana trench, is slightly slower that predicted from ARC-1, the assumption of their lid velocity is not critically examined.

Seekins and Teng [1977] was the first to attempt analyzing regional variation of upper mantle structure, using several events at the perimeter of the Philippine Sea plate recorded at GUMO (Guam). However, since they used a limited number of events and also assumed a poor regionization, it is not straightforward to interpret their observation in terms of regional variation. *Shiono et al.* [1980] used "pure path" analysis to compare older and younger Philippine Sea plate, west and east of Kyushu-Palau ridge, respectively, and showed that the younger eastern side has a lower group velocity and interpreted this with a cooling plate model.

The most extensive study on group velocity dispersion and its lateral variation was performed by *Oda and Senna* [1994] who showed that average group velocity in the entire Philippine Sea Plate is slightly lower than ARC-1 prediction in the 30-80 sec band. As for the regional variation, their observed group velocities for the western Philippine basin were

slightly higher than this average, interpreted to represent the older, thus thicker, lithosphere there.

However, recent numerical experiments by *van Heijst, Snieder, and Nowack* [1994] revealed that, with the presence of a low-velocity zone, group velocity dispersion data cannot determine the velocity structure uniquely unless intermediate and deep events are included, which is analogue to the non-uniqueness of body-wave travel times. Since a negative reflectivity at the G discontinuity found by *ScS* study implies the existence of a low-velocity zone as is commonly observed in oceanic regions, their finding limits the direct comparison between previous models and PHB3.

On the other hand, their observed group velocity dispersion curves can be used as independent data to test our model. Since PHB3 is a path-averaged, one-dimensional model, it is preferable to compare our prediction with previous observations for the most similar paths to minimize lateral variations of dispersion [*Oda and Senna*, 1994]. We chose the data of *Shiono et al.* [1980] for the western Philippine Basin, whose observations sampled the same corridor as ours do (Fig. 4.6). Fig. 4.7 shows their observation and our prediction. Although their model WPL50 has an assumed typical lid velocity [*Dorman et al.*, 1960] and consequently the *S*-velocity structure is different from our model PHB3 (Fig. 4.8), our predicted group velocities fit their observations well within the scatter of their data (± 0.10 km/s and ± 0.20 km/s for Rayleigh and Love waves, respectively) in the 30-80 sec band. Our PHB3 prediction shows that group velocities of the first two branches are close to that of the fundamental mode branch and this might account for the misfit of Rayleigh wave dispersion at short periods. This shows that their dispersion cannot reject our model, which indicates that our model is consistent with previously proposed models.

As for the transition zone structure, *Chen and Nowack* [1994] recently found that *P*-velocity in the transition zone beneath Philippine Sea is high, which they attributed to the subducted slab. Their result is in consistent with the high *S*, therefore *P* velocities in the

transition zone in PHB3. At this stage, we cannot measure phase delays of such phases as *P*, *pP*, and *PP* because of the difficulty constructing isolation filter with normal-mode theory. Inclusion of direct measurement of *P*-velocity is a logical next step in improving this methodology.

Table 4.1 Model PHB3

Depth km	v_{SH} km/s	v_{SV} km/s	v_{PH} km/s	v_{PV} km/s	ρ kg/m^3	η
0.0	0.00	0.00	1.50	1.50	1.03	1.00
5.4	0.00	0.00	1.50	1.50	1.03	1.00
5.4	0.92	0.92	2.10	2.10	1.50	1.00
5.5	0.92	0.92	2.10	2.10	1.50	1.00
5.5	3.48	3.48	6.27	6.27	2.83	1.00
16.9	3.48	3.48	6.27	6.27	2.83	1.00
16.9	4.54	4.39	8.02	7.91	3.28	0.91
51.0	4.54	4.39	8.02	7.91	3.28	0.91
51.0	4.59	4.41	8.14	8.00	3.35	0.91
89.3	4.59	4.41	8.14	8.00	3.35	0.91
89.3	4.43	4.22	8.05	7.89	3.35	0.91
165.5	4.31	4.23	8.07	7.99	3.35	0.94
165.5	4.27	4.27	8.03	8.03	3.35	1.00
407.7	5.27	5.27	9.76	9.76	3.87	1.00
407.7	5.12	5.12	9.36	9.36	3.76	1.00
520.4	5.27	5.27	9.76	9.76	3.87	1.00
520.4	5.34	5.34	9.77	9.77	3.88	1.00
664.0	5.57	5.57	10.22	10.22	4.02	1.00
664.0	5.78	5.78	10.66	10.66	4.35	1.00
761.3	6.16	6.16	10.94	10.94	4.42	1.00
761.3	6.19	6.19	11.02	11.02	4.44	1.00
771.0	6.22	6.22	11.05	11.05	4.44	1.00

FIGURE CAPTIONS

Fig. 4.1 Final model PHB3. From left to right, η, density, shear velocities, and the compressional velocities are plotted as a function of depth. The model is radially anisotropic through the lithosphere and the low-velocity zone, with v_{SH} and v_{PH} being higher than v_{SH} and v_{PV}, respectively. Below 771 km depth, PHB is identical to PREM.

Fig. 4.2 Comparison of observed and predicted *ScS* reverberation data. Top one is for reflectivities, and the bottom one is for the vertical travel times. Solid symbols represent the residual relative to observation of *Revenaugh and Jordan* [1991c], and the lines represent the predicted fit. Size of error bars are calculated by a weighted average of estimated *a priori* errors. Note that PHB3 does not satisfy observed reflectivity at Moho, but otherwise the fit is good.

Fig. 4.3 Comparison of observed and predicted frequency-dependent travel time data. Phase delays are categorized by phase type (Surface wave, *SS*, or *S*), and then separated into tangential (*SH*) or radial/vertical (*SV*) observations, and averaged in each frequency band. Symbols represent the residuals relative to PHB, while the lines represent the predicted fit of model PHB3 to these data. Dispersion relative to PHB is indicated by a frequency-dependent trend, while evidence of anisotropy can be observed as a separation of the *SH* and *SV* observations for a given phase type. a) Love and Rayleigh waves. b) *SSS* and *sSS* waves. c) *SS* waves. d) *S* waves. Magnitudes of error bars are calculated by a weighted average of estimated *a priori* errors.

Fig. 4.4 Comparison of observed and synthetic seismograms from all 28 events used in the inversion. Waveforms are plotted according to their epicentral distances from station MAJO, and for each pair, the top trace is the data and the bottom trace is the synthetic

seismogram, complete to 50 mHz. Both traces are filtered between 5 and 45 mHz. Traces are roughly aligned on *S* phase at 0 min.

Fig. 4.5 Comparison of model ARC-1 [*Kanamori and Abe,* 1986], and model PHB3. ARC-1 is modeled to fit observed Rayleigh wave group velocity dispersion curve, sampling Philippine Sea.

Fig. 4.6 Events used in our inversion (Fig. 1.1), and used by *Shiono et al.* [1980] for model WPL50.

Fig 4.7 Comparison of predicted group velocity for model WPL50 [*Shiono et al.,* 1980], and predicted group velocity of fundamental mode for PHB3. Observations of *Shiono et al.* [1980] are scattered (± 0.10 km/s and ± 0.20 km/s for Rayleigh and Love waves, respectively) in the 20-80 sec around their prediction and our prediction i

Fig. 4.8 Comparison of model WPL50 [*Shiono et al.,* [1980] and model PHB3. WPL50 is indirectly using ARC-1 as initial model through models of *Seekins and Teng* [1977], and its lid velocity is the same value given by *Dorman et al.* [1960].

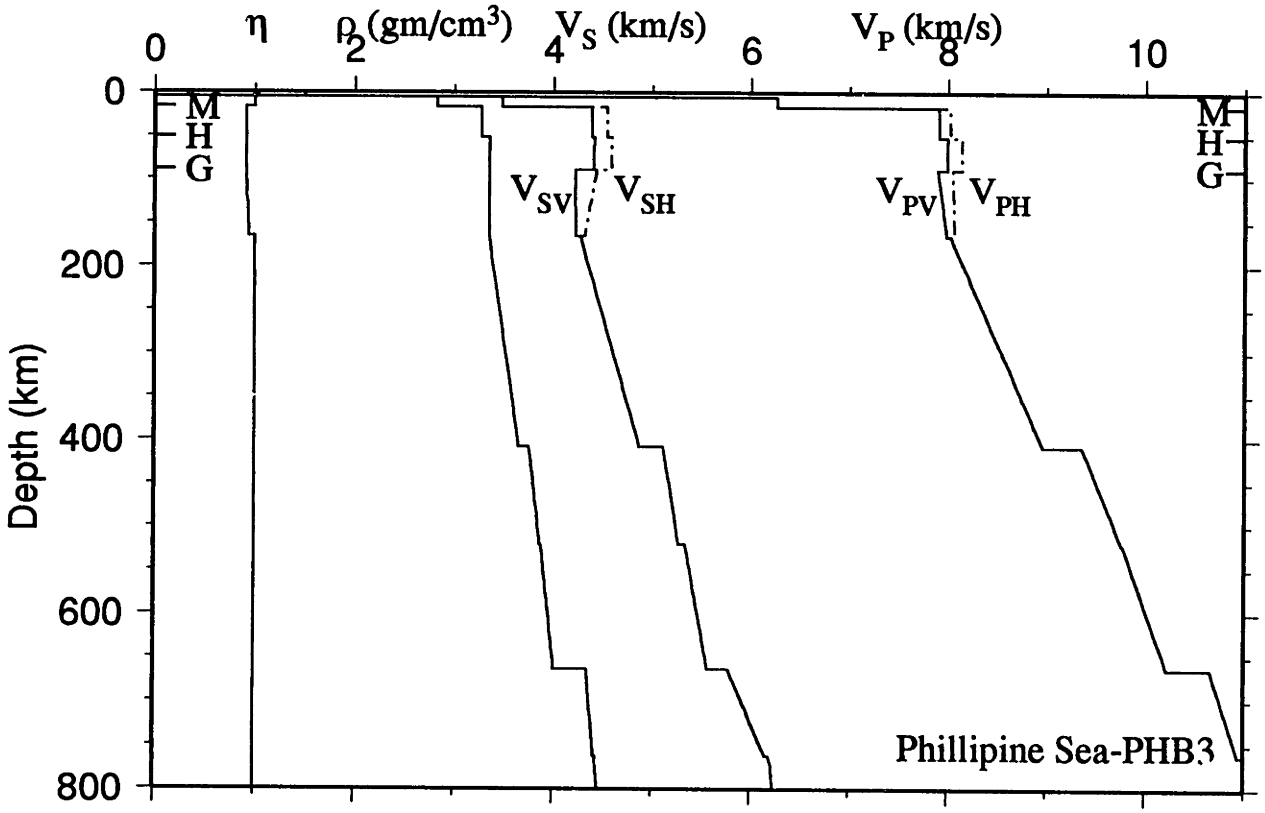
η
ρ (gm/cm³)
V_S (km/s)
V_P (km/s)
0
2
4
6
8
10
0
200
400
600
800
Depth (km)
M
H
G
V_SV
V_SH
V_PV
V_PH
M
H
G
Phillipine Sea-PHB3

Figure 4.1

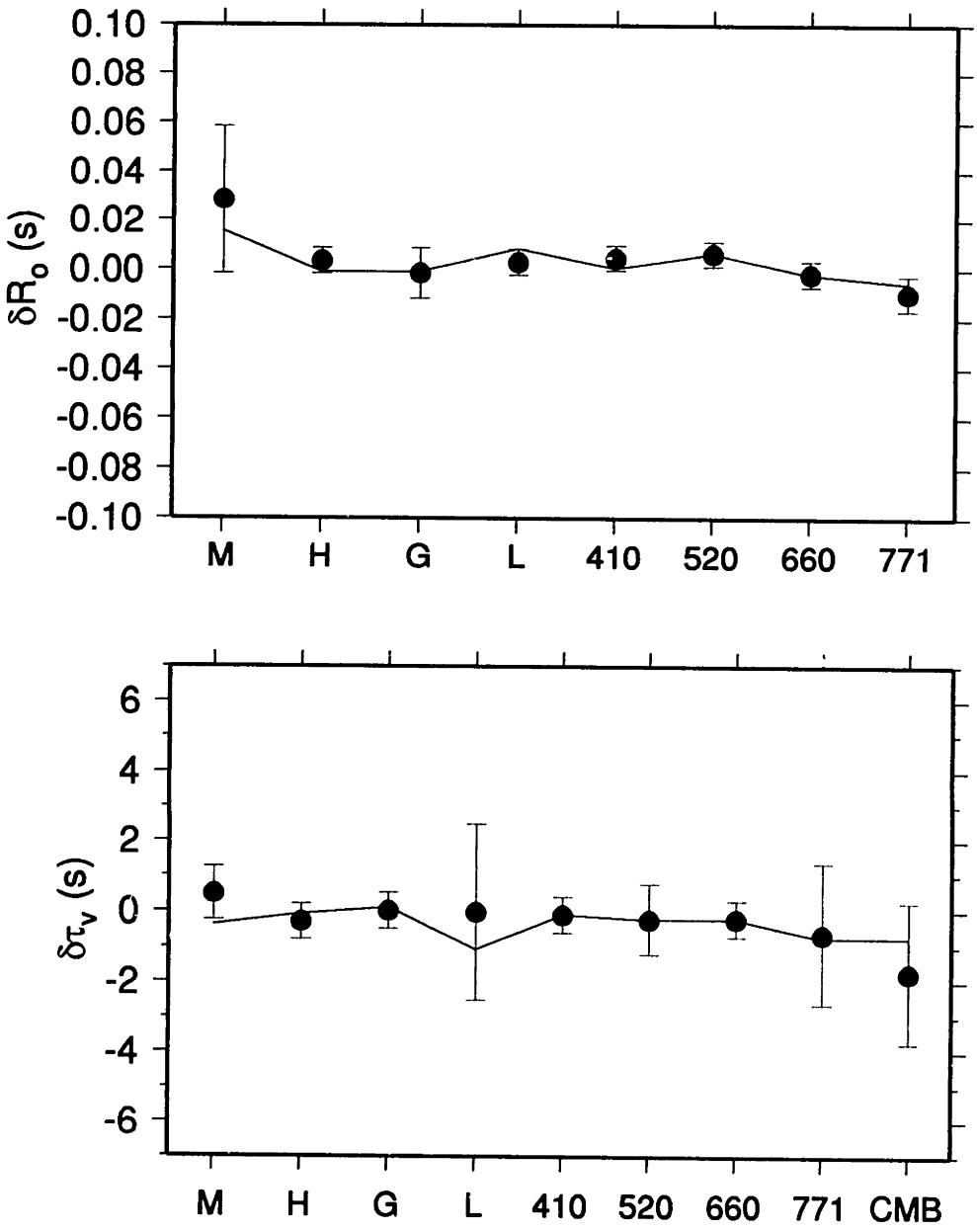
0.10
0.08
0.06
0.04
0.02
0.00
-0.02
-0.04
-0.06
-0.08
-0.10
δR_o (s)
M
H
G
L
410
520
660
771
6
4
2
0
-2
-4
-6
δτ_v (s)
M
H
G
L
410
520
660
771
CMB

Figure 4.2

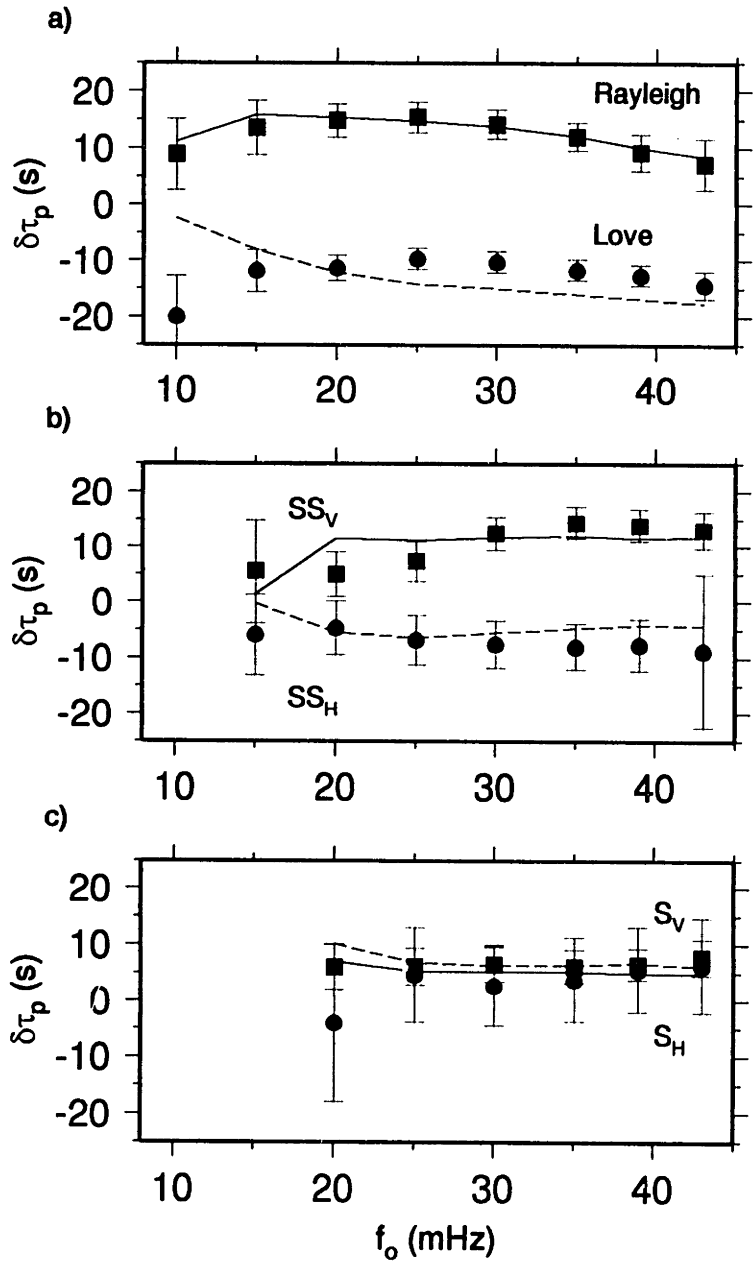
a)
Rayleigh
Love
b)
SS_V
SS_H
c)
S_V
S_H
$\delta\tau_p$ (s)
20
10
0
-10
-20
10
20
30
40
f_o (mHz)

Figure 4.3

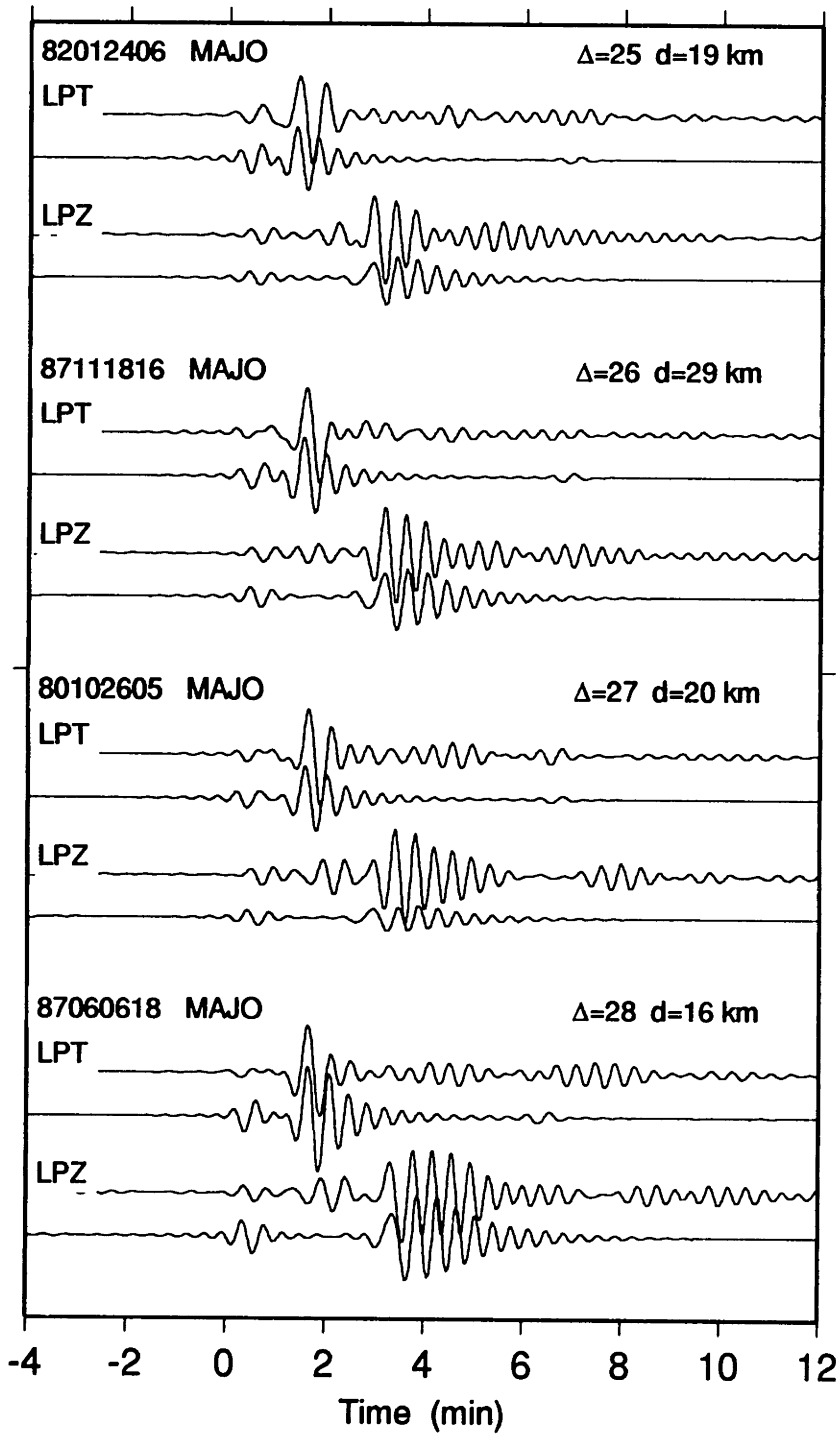
82012406 MAJO
Δ=25 d=19 km
LPT
LPZ
87111816 MAJO
Δ=26 d=29 km
LPT
LPZ
80102605 MAJO
Δ=27 d=20 km
LPT
LPZ
87060618 MAJO
Δ=28 d=16 km
LPT
LPZ
-4
-2
0
2
4
6
8
10
12
Time (min)

Figure 4.4a

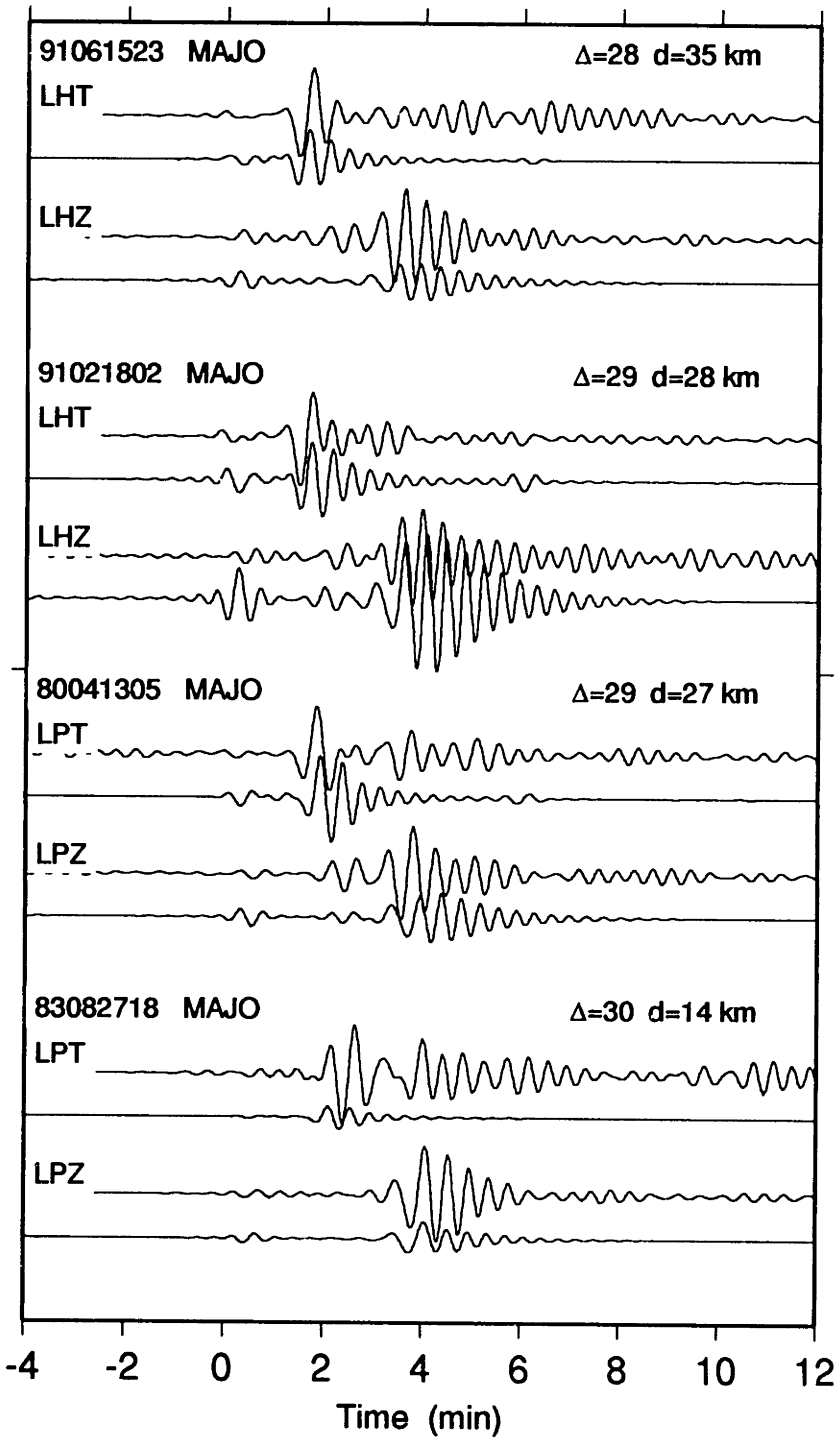
91061523 MAJO
Δ=28 d=35 km
LHT
LHZ
91021802 MAJO
Δ=29 d=28 km
LHT
LHZ
80041305 MAJO
Δ=29 d=27 km
LPT
LPZ
83082718 MAJO
Δ=30 d=14 km
LPT
LPZ
-4
-2
0
2
4
6
8
10
12
Time (min)

Figure 4.4b

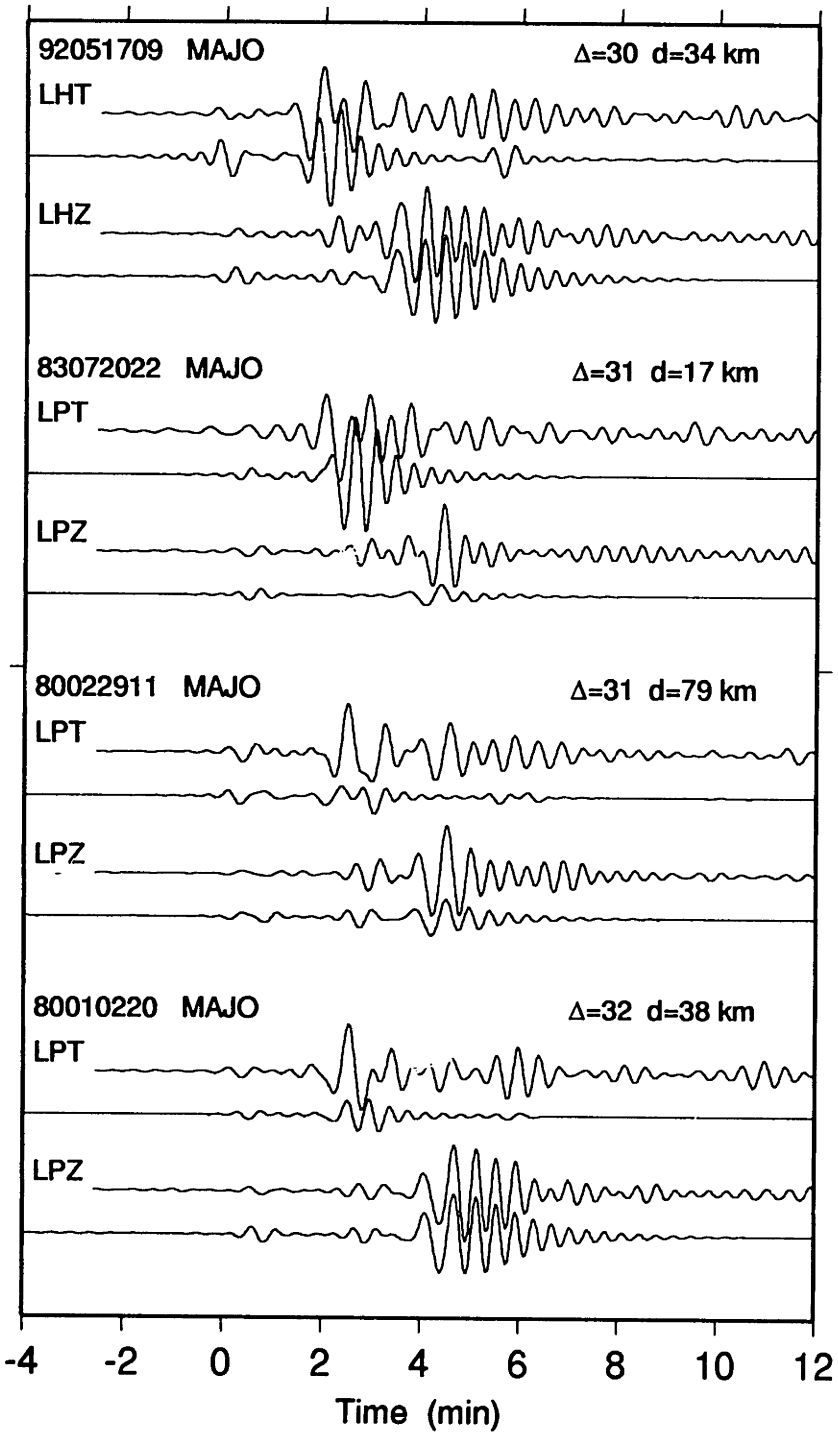
92051709 MAJO
Δ=30 d=34 km
LHT
LHZ
83072022 MAJO
Δ=31 d=17 km
LPT
LPZ
80022911 MAJO
Δ=31 d=79 km
LPT
LPZ
80010220 MAJO
Δ=32 d=38 km
LPT
LPZ
-4
-2
0
2
4
6
8
10
12
Time (min)

Figure 4.4c

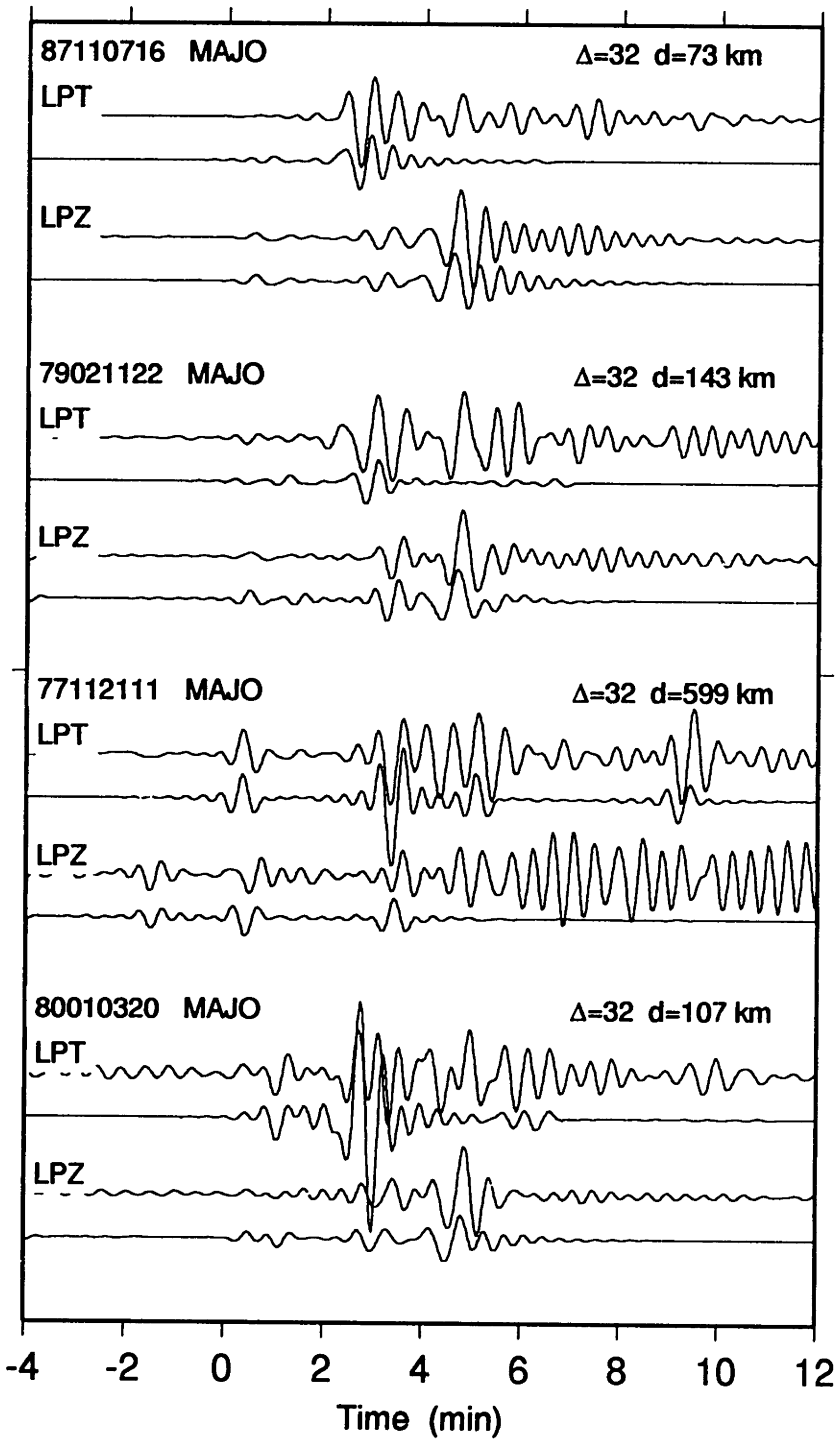
87110716 MAJO
Δ=32 d=73 km
LPT
LPZ
79021122 MAJO
Δ=32 d=143 km
LPT
LPZ
77112111 MAJO
Δ=32 d=599 km
LPT
LPZ
80010320 MAJO
Δ=32 d=107 km
LPT
LPZ
-4
-2
0
2
4
6
8
10
12
Time (min)

Figure 4.4d

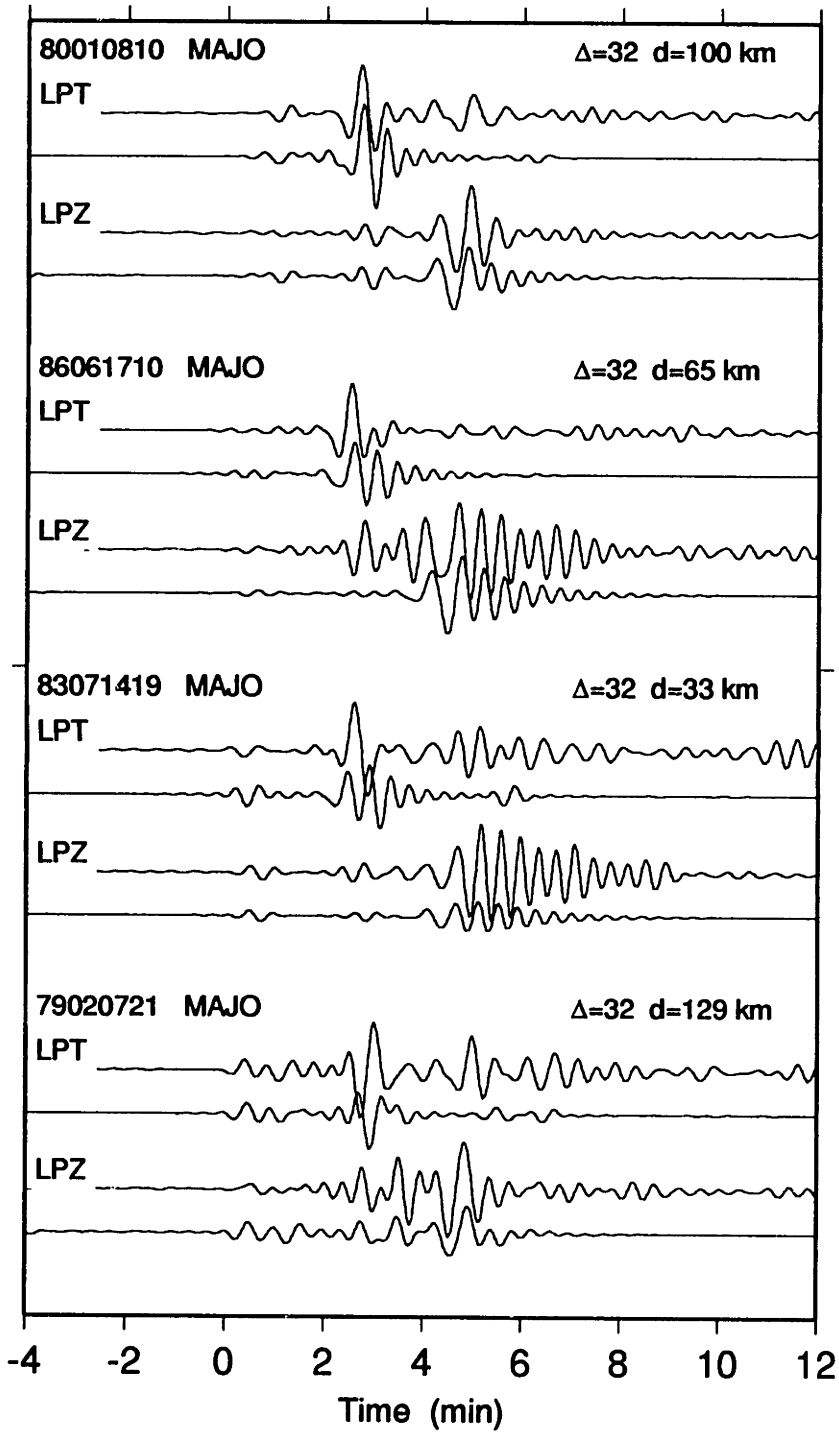
80010810 MAJO
Δ=32 d=100 km
LPT
LPZ
86061710 MAJO
Δ=32 d=65 km
LPT
LPZ
83071419 MAJO
Δ=32 d=33 km
LPT
LPZ
79020721 MAJO
Δ=32 d=129 km
LPT
LPZ
-4
-2
0
2
4
6
8
10
12
Time (min)

Figure 4.4e

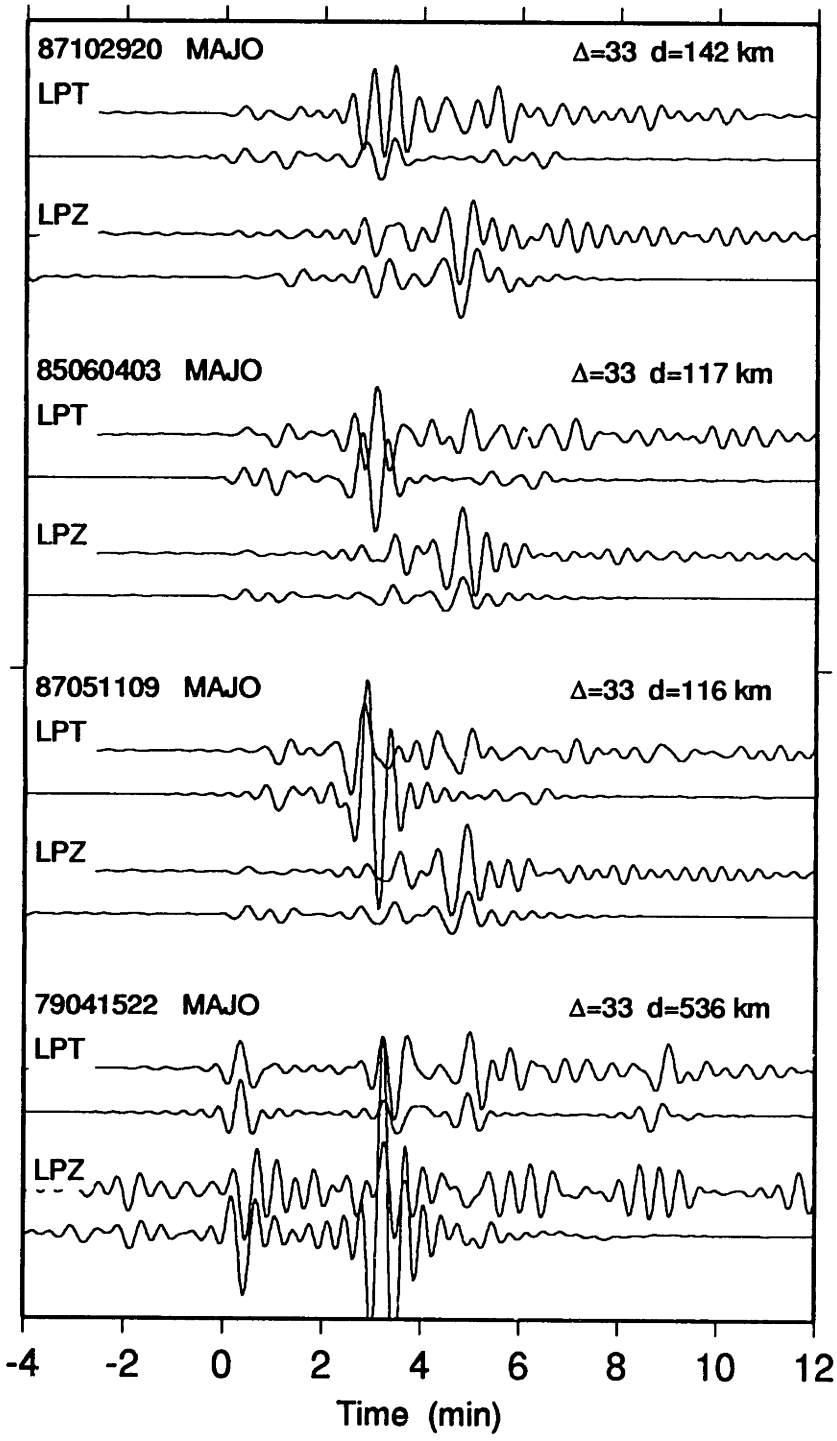
87102920 MAJO
Δ=33 d=142 km
LPT
LPZ
85060403 MAJO
Δ=33 d=117 km
LPT
LPZ
87051109 MAJO
Δ=33 d=116 km
LPT
LPZ
79041522 MAJO
Δ=33 d=536 km
LPT
LPZ
-4
-2
0
2
4
6
8
10
12
Time (min)

Figure 4.4f

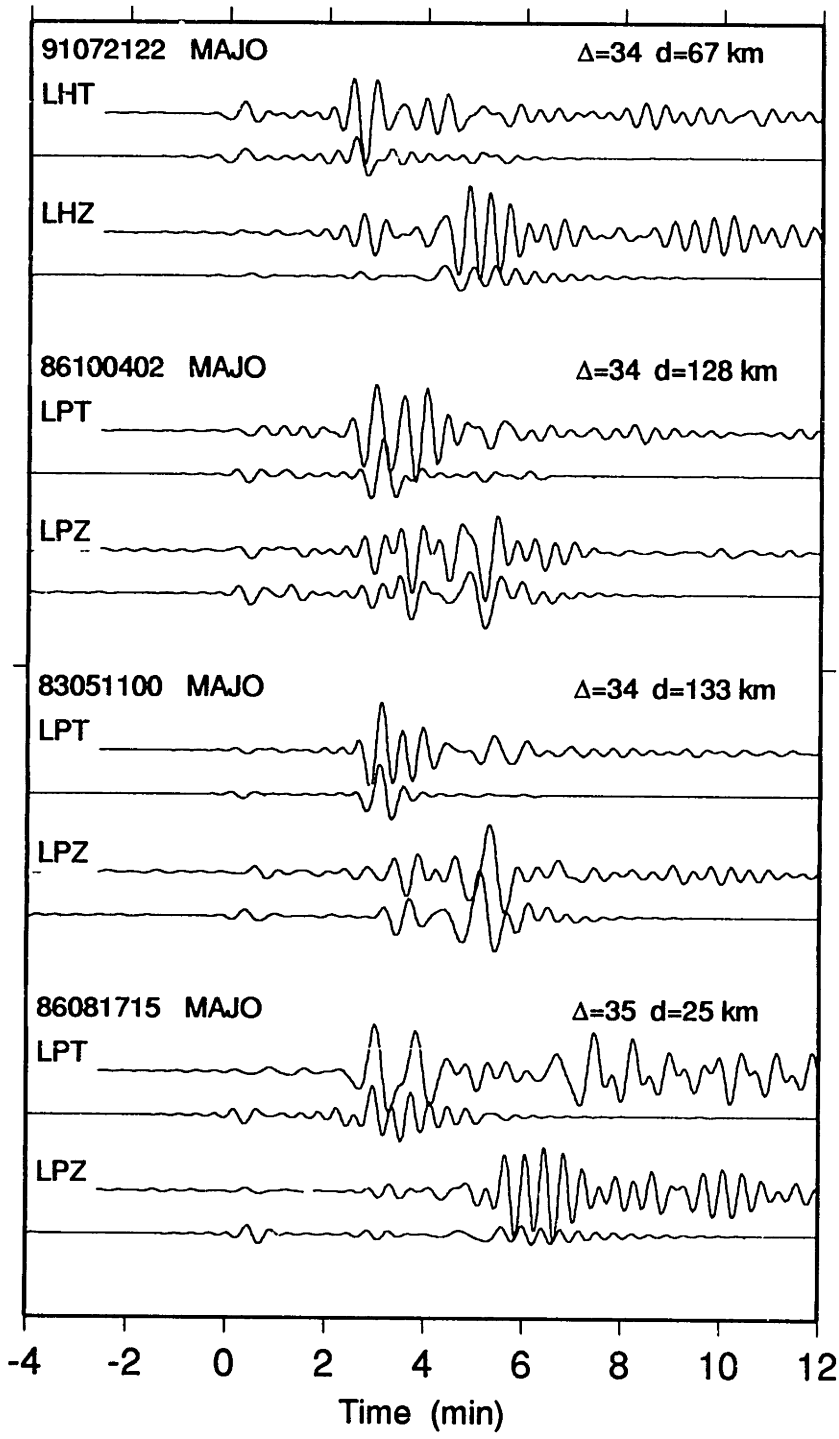
91072122 MAJO
Δ=34 d=67 km
LHT
LHZ
86100402 MAJO
Δ=34 d=128 km
LPT
LPZ
83051100 MAJO
Δ=34 d=133 km
LPT
LPZ
86081715 MAJO
Δ=35 d=25 km
LPT
LPZ
-4
-2
0
2
4
6
8
10
12
Time (min)

Figure 4.4g

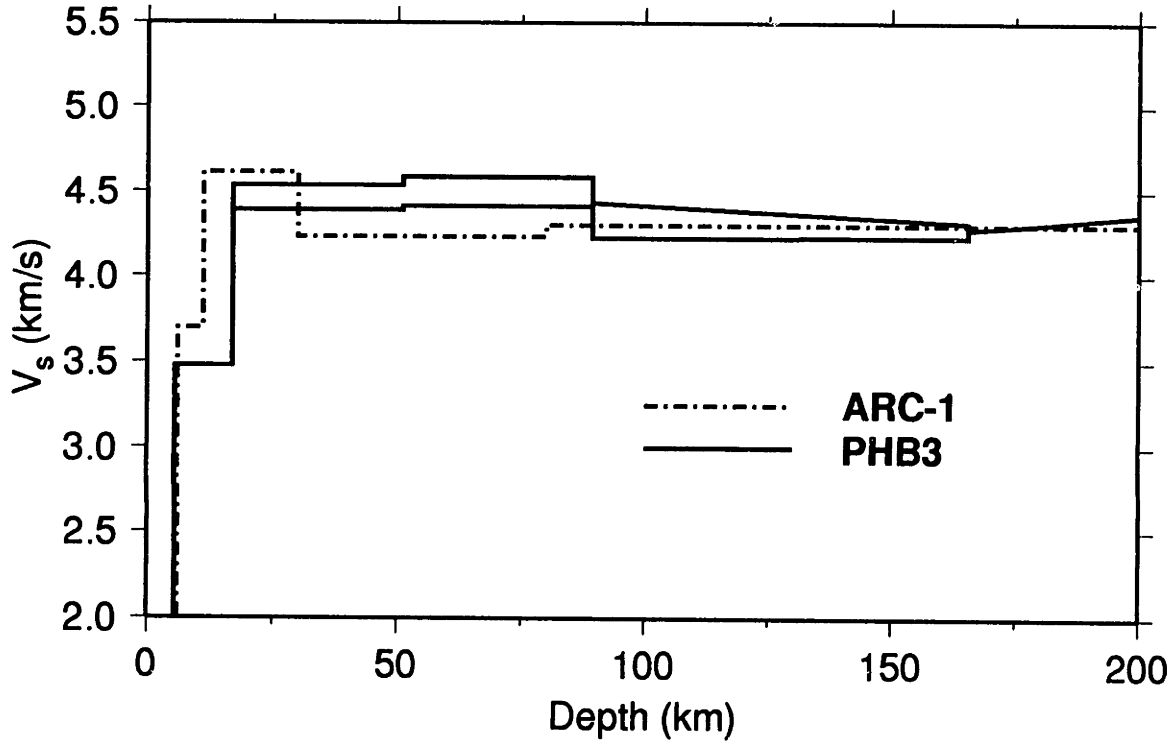

Figure 4.5

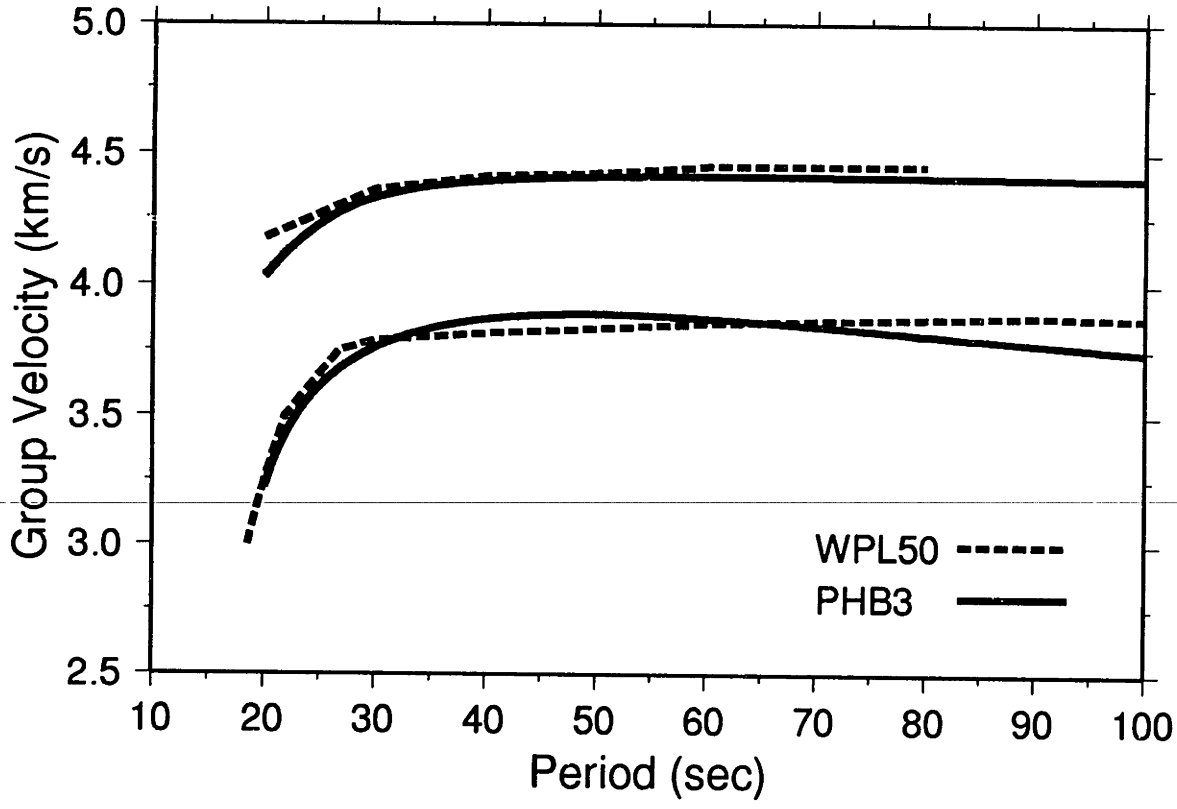
5.0
4.5
4.0
3.5
3.0
2.5
Group Velocity (km/s)
10
20
30
40
50
60
70
80
90
100
Period (sec)
WPL50
PHB3

Figure 4.6

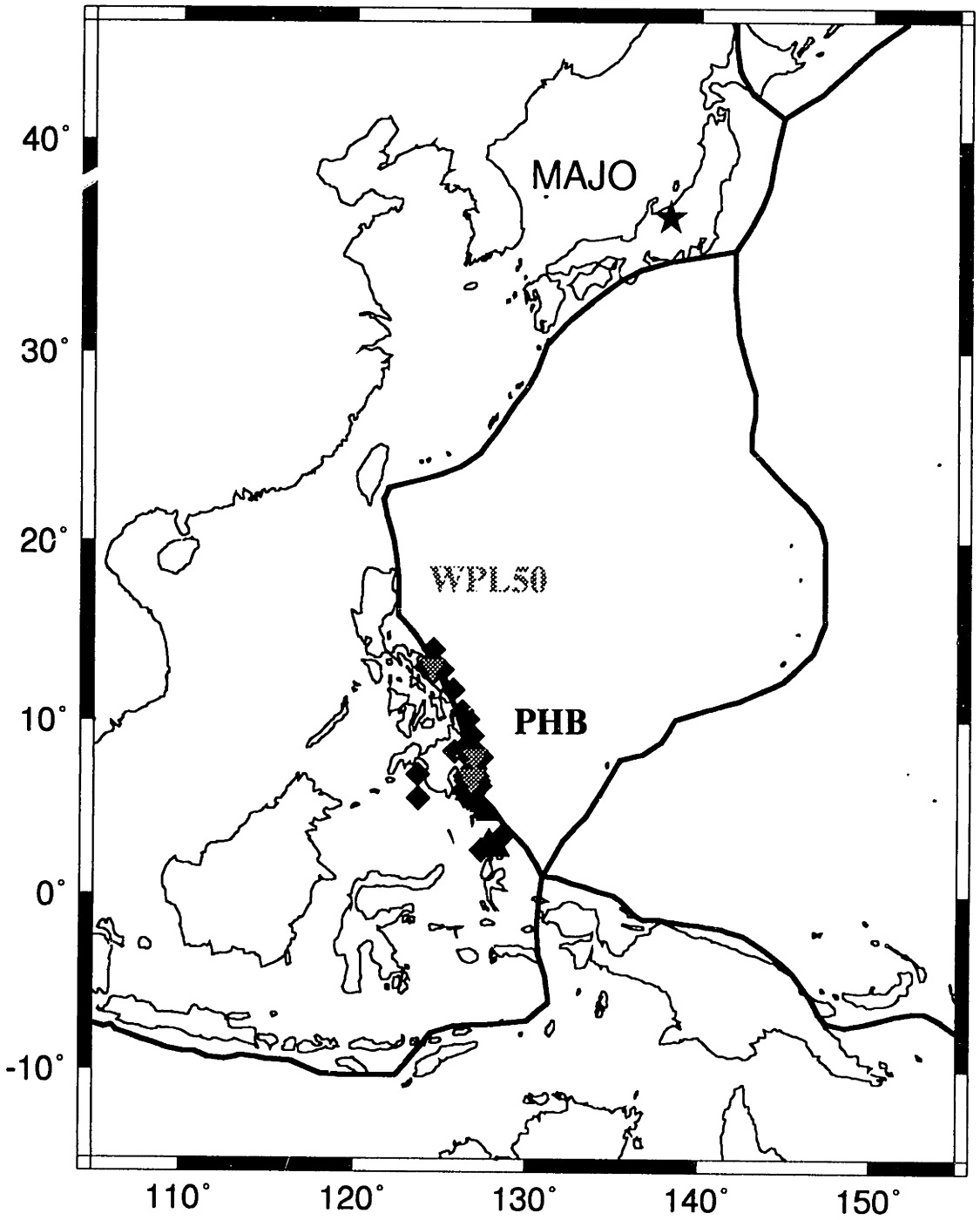

Figure 4.7

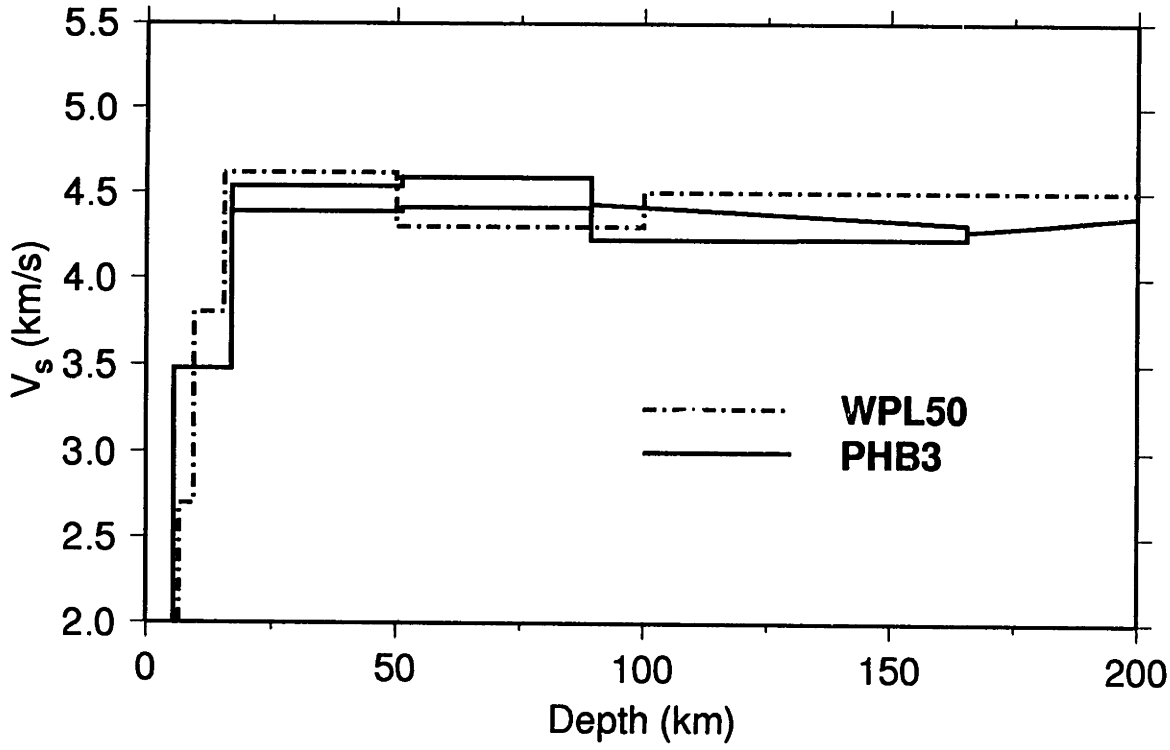

Figure 4.8

Chapter 5: Discussion

In this chapter we discuss the characteristics of the model PHB3 presented in the last chapter. Among the main issues are the thick crust, and the thick lid.

5.1 Crustal thickness

From refraction experiments, *Murauchi et al.* [1968] concluded that the average crust thickness in the Philippine Sea did not differ much from the Pacific plate seafloor of similar ages, which is 6 to 7 km. On the other hand *Louden* [1980] suggested that the crust is about 1 km thinner in the western Philippine Basin (Fig. 1.1), also from marine seismological experiments. *Revenaugh and Jordan* [1991a] concluded 15 km as their best estimate for this corridor and related this to the existence of aseismic Kyushu-Palau ridge in the corridor, where thicker crust (~15 km) was found by refraction experiments [*Murauchi et al.*, 1968]. Thick crust in Amami Plateau and its vicinity was also suggested by *Oda and Senna* [1991] to explain regionized group velocity dispersion observation. Our best estimate is slightly thinner than that of *Revenaugh and Jordan* [1991a] but still thicker than a normal oceanic crust. Our experiments showed that a crustal thickness less than 10 km was possible only at the expense of fit to *R* phase delay data and an (unlikely) large perturbation of *S* velocity in the crust. The change of gradient of Rayleigh wave group velocity around 25 sec (Fig. 4.7), as well as the group velocity itself at shorter periods, is closely related to the crust structure. *Shiono et al.* [1980] modeled a thick crust (a 3 km thick upper crust with v_S = 2.7 km/s and a 6 km thick lower crust with v_S = 3.8 km/s) to explain these observations. Therefore a thicker crust seems be preferred to explain path-averaged long-period observation.

The coverage by marine seismological surveys is still sparse in this complex tectonic region, and the lateral variation of the crustal structure has not yet been fully

explored. *Katzman and Jordan* [1995] recently initiated a new style of tomography, in which zeroth- and first-order *ScS* reverberations are used to model both velocity perturbation and lateral variation of major discontinuity depths. However, their method is not yet be applicable to the variation of the crust thickness along the path, and development of new method that takes into account the along-path variation of shallow structure is necessary to clarify this question.

5.2 Lid velocity and thickness

A thick lid, as reported in *Revenaugh and Jordan* [1991b], remained in the final model. In addition, its *S* velocities are lower than the typical value for the oceanic mantle. Compared to the model PA5 [*Gaherty*, 1995], which has a high velocity lithosphere (v_{SV}= 4.65 km/s) bounded by the G discontinuity located at 68 km, you can clearly see the difference of the shear velocity and the lid thickness (Fig. 5.1). Considering the age difference, 125 Ma in the Pacific versus 50 Ma in the Philippine Sea, it is not a straightforward comparison, however. Moreover, while the difference of the velocity is in the right direction, slower in the younger region, the difference of thickness is in the opposite one, thicker in the younger region.

Thermal model of the lithosphere

Since observed heat flow in the Philippine Sea is slightly higher than but compatible to that in the Pacific throughout the ages [*Sclater et al.*, 1976] and the slope of the of age-bathymetry curve is similar [*Park et al.*, 1990], a large difference of the thermal structure between two regions is very unlikely. The difference of the average lithosphere temperature is about 160 K between the sea floor and 100 km depth, when we used a half-space cooling model and assumed seafloor age of 100 Ma and 50 Ma for each region, respectively.

Using regional velocity models of *Nishimura and Forsyth* [1989], we obtained the temperature derivative of shear velocity $\partial v_S/\partial T$ -0.52 m $s^{-1}K^{-1}$ (Fig. 5.3). This value is comparable to the previous estimate, -0.62 m $s^{-1}K^{-1}$ [*McNutt and Judge,* 1990], and is also consistent with $\partial v_P/\partial T$ = -0.5 m $s^{-1}K^{-1}$ [*Creager and Jordan,* 1986; *Fisher et al.,* 1988] if we assume $\partial v_S/\partial T$ =1.1 $\partial v_P/\partial T$ [*Woodhouse and Dziewonski,* 1984]. We could not fit the slow velocity in the youngest region linearly but we speculate that this is due to the existence of partial melt, or the temperature close to the mantle solidus [*Sato et al.,* 1989]. Therefore, a thermal model predicts only half of the observed 0.25-0.3 km/s difference of lithosphere *S* velocity between PA5 and PHB3. Moreover, no thermal model gives a thicker lithosphere for a younger region. For example, a half-space model gives thicknesses for the thermal boundary layer (TBL) of about 110 km and 80 km for PA5 and PHB3, respectively. Therefore we speculate this compositional variation is required to explain this difference.

Compositional variation in the lithosphere

The Philippine Sea plate is primarily characterized by its back-arc spreading origin [*Seno and Maruyama,* 1984; *Hall et al.,* 1995], and it is plausible that our findings of thick, low-velocity seismic lid is attributed to the different type of plate genesis. Particularly notable is that in our model PHB3, which has a thick lithosphere, the crust is also thick. This positive correlation between the lithosphere and the crust thickness suggests that this structure could be related to the evolution of the upper mantle, specifically the process of the crust production. Depletion of basalt changes the chemistry of the residue, and difference of the lithosphere structure might be the expression of the compositional variation. Difference of seismic velocities in the mantle then might be an expression of compositional variation of major element chemistry, namely Mg number, and/or minor element chemistry, especially volatile content.

The basalt depletion increases the Mg number in the residuum, which is the molar ratio Mg/(Mg+Fe). When the basalt is subtracted from the primitive mantle, the resultant higher Mg number lowers the density and increases velocity compared to the primary mantle [*Jordan*, 1979]. This less denser residue material would float above the primary mantle and be maintained there as a chemical boundary layer (CBL). The thickness of this CBL is controlled by the amount of subtracted basalt (crust). If there is a difference of the crust production between two regions, the thickness of this CBL could be different. In our case, the Philippine Sea upper mantle probably experienced the basalt subtraction twice; first at the stage of original plate genesis, and second during the back-arc spreading, while the Pacific upper mantle experienced that only once at the mid-ocean ridge.

Nevertheless, the spreading events were associated with the interaction among surface plates, the subducting slab, and the asthenospheric flow [*Tamaki and Honza*, 1991; *van der Hilst and Seno*, 1994], and it is unlikely that the original CBL, which is the byproduct of the initial basalt depletion, stayed in the vicinity of the spreading center and grew vertically. The basaltic melt is probably supplied by the undepleted upper mantle driven into by either a passive or an active flow, and CBL is likely to grow rather laterally as is in the mid-ocean ridge. Further, a basalt depletion will increase the *S*-velocity, though its magnitude is not as large as the density counterpart, and this requires a larger $\partial v_S/\partial T$ than our estimate above. Therefore it is unlikely that a variation of major elements explains the difference of the observed lid structure successfully.

Hirth and Kohlstedt [1995] recently presented a model that the dry melted mantle (lithosphere) overlays the wet unmelted mantle (asthenosphere), from the laboratory experiments that show the viscosity of olivine aggregates drops an order of magnitude in the present of water [*Karato et al.*, 1986], and that solubility of water in the basaltic melt is at least a couple of orders larger than that in olivine at a high pressure [*Karato*, 1986]. In this compositionally stratified model, the lithosphere-asthenosphere boundary represents the compositional boundary, which becomes a mechanically decoupled zone.

When we assume that the G discontinuity is the seismic representation of this boundary, the deeper G discontinuity in the western Philippine Sea then implies that at the initial stage of the plate evolution the melting depth was deeper than that in the Pacific. Because the subducting slab brings volatiles including water into the upper mantle [*Peacock,* 1990], a higher water content of back-arc mantle is very likely. Because the solidus of the wet peridotite is lower than that of the dry peridotite [*Ringwood,* 1975], the larger amount of water enhances the melting of the mantle and, as a result, the compositional boundary becomes deeper. The presence of water in the upper mantle reduces the *S* velocity from that of the dry mantle [*Karato,* 1995]. If the amount of water is large enough to saturate the basaltic melt, the *S* velocity in the wet lid (though much dryer than the asthenosphere) could be lower than a thermal model prediction. The abundance of water also might explain the slightly lower *S* velocities in the low-velocity zone in the western Philippine Sea.

Thickness of the seismic lid does not coincide to that of thermal lithosphere, but that of mechanical lithosphere in the Pacific [*Gaherty et al.,* 1996]. The depth to this compositional boundary is not a function of local lithospheric temperature [*Sato et al., 1989*] and the G discontinuity does not deepen as plate becomes older. Therefore, the observed positive correlation between the surface wave velocity and the lithospheric age [*Nishimura and Forsyth,* 1989; *Zhang and Tanimoto,* 1992] would have to be explained mostly by the *S* velocity of the lid and the low-velocity zone.

Our model does not explain the sea depth anomaly for the Phi'ippine Sea, nor does it have to. For example, *Sclater et al.* [1976] explained the unusual sea depth with slightly positive free-air anomaly in the Western Philippine Basin and Shikoku Basin [*Watts and Bodine,* 1978] with a thinner oceanic crust and a "normal" lithosphere. The Philippine Sea plate is surrounded by subduction zones and part of this bathymetry anomaly could be explained by the dynamic topography caused by subducting slabs. *Louden* [1980] suggested that remnant of ancient subducted slab [*van der Hilst and Seno, 1994*] might

explain the bathymetry anomaly, which as we will discuss below seems in agreement with our model that is characterized by higher velocities in the transition zone.

5.3 From low-velocity zone to transition zone

The depth of L discontinuity, where the gradients change, had a significant effect on waveforms. Prior to this particular series of modeling, we experimented a series of similar inversion using different initial models, and the results showed that the thick lid and upper mantle structure are likely to exist in the western Philippine Sea [*Kato and Jordan*, 1994]. In prior experiments, however, we started with L discontinuity deeper than 200 km and the preferred final models had an isotropic low-velocity zone with positive velocity gradient bounded at L discontinuity between 200 and 220 km. When L discontinuity was deep, we had a difficulty matching transverse-component waveforms, especially Love waves, although it was possible to get a reasonable waveforms in both vertical and radial components. It should be noted that because of non-linearity between lid-low velocity zone structure and waveforms of Love wave, it was difficult to change the depth of L discontinuity during inversion of phase-delay data. This example shows the difficulty of modeling complex waveforms, especially transverse component, at regional distances, and the importance of a good initial model. We obtained a better fit to all three components with a shallower L discontinuity (~160 km), although we still have trouble with some events.

A small discontinuity at the L discontinuity appears in PHB3, but the reflectivity is probably below the detection level of the *ScS* reverberations, and the model does not disagree with the result of *Revenaugh and Jordan* [1991c]. This could be an artifact of our model parameterization and therefore can be removed by a smoother parameterization. However, an additional reflectivity peak might improve the fit between their observed and predicted reflectivity profile (Fig. 2.1) [*Revenaugh and Jordan*, 1991c], and since a large positive reflectivity in the corridor intersecting our corridor in the western Philippine Sea

(Chapter 2), we cannot completely rule out the existence of an L discontinuity in this region.

The steep velocity gradient between the L discontinuity and 410-km discontinuity of PHB3 is very close to that of PA5 [*Gaherty,* 1995], despite their differences in the shallow parts of the mantle. The steep velocity gradients in this depth range, which appears in many previous models [e.g. *Grand and Helmberger,* 1984; *Lerner-Lam and Jordan,* 1987] appear to be a well resolved feature of the oceanic upper mantle [*Gaherty et al.* , 1996].

Depths of two major discontinuities in the transition zone are anti-correlated between PHB3 and PA5. PHB3 has a shallower 410-km and deeper 660-km discontinuity than PA5 does, and this observation agrees with the finding of *Revenaugh and Jordan* [1991c]. If these discontinuities result from simple phase changes (and no compositional change), then their depths imply that the transition zone in the western Philippine Sea is colder than that in the Pacific. This high velocity in the transition zone is also found in global tomographic models, such as model S12 [*Su et al.,* 1994] (Fig. 5.3), as well as in recent delay time tomography models [*Fukao et al.,* 1992], and *van der Hilst et al.,* 1991]. *Tajima and Grand* [1995] studied waveforms of initial *P* phases of deep events in the Kurils and showed that a faster transition zone with deeper 660-km discontinuity explained observed triplication very well. Although the geographical location of our study is different from theirs, these two regions share a common geophysical environment, and both show high velocity anomalies in the transition zone in tomographic models [*Fukao et al.,* 1992; *van der Hilst et al.,* 1991]. This implies that the velocities in the transition zone reflects the subduction events in the past. This relation between the surface and tectonics and the velocity structure in the transition zone needed to be examined in other regions.

The observed reflectivity at 660-km discontinuity in the Pacific is larger (7.8%) than that in the western Philippine Sea (5.8%) [*Revenaugh and Jordan,* 1991b]. The magnitude of *S* velocity jump at 660-km discontinuity in PA5 is much (almost three times) larger than that in PHB3, although both models provide a good fit to the observed

reflectivities, which are also functions of the density increase. This structure could be biased by the assumption that the lower mantle of PHB3 is identical to PREM, and our data has a limited resolution of this structure. Hence, we cannot conclude that the *S* velocity jump is smaller when 660-km discontinuity is deeper. Possible contribution of a phase change of garnet species in this depth to the reflectivity and the depth [e.g. *Ita and Stixrude*, 1993] makes it difficult to interpret the relation between the fine-structure reflectivity and apparent depth in the low-frequency (~35 mHz) observations [*Revenaugh and Jordan*, 1991b]. Corroboration between mineralogists and seismologists is essential to clarify the nature of this discontinuity.

5.4 Anisotropy

The depth extent of the anisotropic layer in the upper mantle is still an open question [*Gaherty et al.*, 1996]. The depth extent of anisotropy in the model of *Nishimura and Forsyth* [1989], who used a smooth parameterization, is much deeper (> 200 km) in regions of comparable sea floor age. Our phase delay data required anisotropy in the low velocity zone, but do not strongly require anisotropy below the L discontinuity. When we allowed small amount of anisotropy (<1%) between the L discontinuity and 410-km discontinuity, the fit to our phase delay data was not improved significantly. This termination of anisotropy at the L discontinuity agrees well with *Gaherty et al.* [1996] (Fig. 5.1), who suggested that anisotropy in the upper mantle is caused both by frozen aliments of olivine and by the active asthenospheric flow. Our implication that the G discontinuity is the bottom of the mechanical boundary layer is also important in its geodynamical implication, and should be further explored.

Since we assumed a two-layer structure between the G discontinuity and 410-km discontinuity and linear gradients in the layers, we could not explore the velocity structure in much finer scale. Although we cannot rule out a small amount of anisotropy below the L

discontinuity completely until we test this model with different parameterization, we believe the existence of deep anisotropy is unlikely.

Yu and Park [1994] analyzed that appearance of *QL* phase, Love wave converted to coupled mode, is related to the gradient of azimuthal anisotropy of the upper mantle. They interpreted the absence of *QL* phases in the waveforms from Philippine Islands recorded in Japan as an indication either that azimuthal anisotropy in this path is weak or that this region can be radial anisotropic at long-wavelengths. Clearly, our results do not disagree with theirs.

5.5 Future directions

Although we have demonstrated that phase delay measurements using the GSDF technique are very useful for investigating the upper mantle structure in the oceanic region, several new directions need to be explored to obtain a better understanding of the processes in the oceanic upper mantle.

Our phase delay measurements are mostly from *S* waves, and the *P* velocities are only constrained by the Rayleigh waves and SV polarized shear waves, as well as the *a priori* mineralogical information. Further development of isolation filters capable of isolating *P* phases, such as *P* and *PP*, will greatly improve our ability to model the compressional velocity, and will provide a better constrains on the mineralogical models and the regional variations. At the same time, measurements at higher frequencies of both shear and compressional wave data are important in order to model the detailed structure of the transition zone and the discontinuities.

Although our path-averaged, one-dimensional model PHB3 provides a reasonable fit to phase delay measurements and a good fit to reverberation data, the synthetic seismograms do not match the observed waveforms as well as we would like. Surface tectonics of our corridor is clearly laterally heterogeneous, both along and across the corridor and we also expect a quite laterally heterogeneous crustal structure. Being

functions of the temperature the chemical compositions, velocities in the layers could vary laterally (Fig. 5.3), which should be correlated to the undulation of major discontinuities. Recently, *Katzman and Jordan* [1995] has improved the reverberation analysis technique for a along-path two-dimensional structure, which successfully applied to the Tonga-Hawaii corridor where they found a large lateral gradient of shear wave velocity in D" layer. It is a logical next step to pursue a new method which takes account of lateral three-dimensional heterogeneous structure.

We implied the differences among the thicknesses of the thermal, mechanical, and seismic lithospheres in oceanic regions, and, on the contrary to previously assumed [*Taylor and Karner,* 1983], we revealed the different lithospheric structure between the normal oceanic region and the back-arc region. We have not yet approached the questions surrounding the mechanism of the back-arc spreading from this new point of view, which should bring a new insight on the chemical, mineralogical and dynamic processes of the oceanic upper mantle. These process in the oceanic regions might be as complex as in the continental region [*Gaherty and Jordan,* 1995], and we have to keep on exploring on these issues.

FIGURE CAPTIONS

Fig. 5.1 Comparison of models PA5 for the Pacific [*Gaherty,* 1995] and PHB3 for the Philippine Sea.

Fig. 5.2 a) Five V_{SV} models of *Nishimura and Forsyth* [1989]. Star, thick cross, plus, circle, and thin cross represent region 1 (0-4Ma), 2 (4-20Ma), 3 (20-52Ma), 4 (52-110 Ma), and 5 (110+ Ma), respectably, in this and following figures. b) Temperature profile predicted from a cooling half-space model. The upper limit of lithosphere age, 4, 20, 52, 110, and 150 Ma, respectively is used to represent each region. Mantle temperature *Tm* of 1300 K, and thermal diffusivity κ of 1.0^{-6} m^2s^{-1} is used. Note that a cooling half-space model gives a relatively lower temperature than a plate model which fits better the bathymetry, and the temperature of older region is slightly biased. c) Plot of average V_{SV} of the lithosphere verses average temperature. In each model *SV*-velocity was integrated between Moho at 15 km depth and 95 km depth, and then divided by the thickness. Dotted lines represent the best least-square fit for the older four regions, whose slope, $\partial v_S/\partial T$, is -0.52 m $s^{-1}K^{-1}$, which is slightly larger than the estimate of *McNutt and Judge* [1990], -0.62m $s^{-1}K^{-1}$. Our estimate is biased by the choice of the thermal model and by that *Nishimura and Forsyth* [1989]'s use of smooth parameterization, and at the same time *McNutt and Judge* [1990]'s estimate is also biased by their choice of reference model (see text). Note that velocity in the youngest region (0-4 Ma) deviates from the best fit line derived from the older regions, and we speculate this is due to the existence of partial melting at the mid-ocean ridge [*Sato et al.,* 1989].

Fig. 5.3 A slice of global tomographic model S12 [*Su et al.,* 1994] projected in the Philippine Sea corridor. In this slice the velocity in the shallow upper mantle (<200 km

depth) is slightly slower than the global average PREM, but is slightly higher in the transition zone. This model is consistent with our model PHB3.

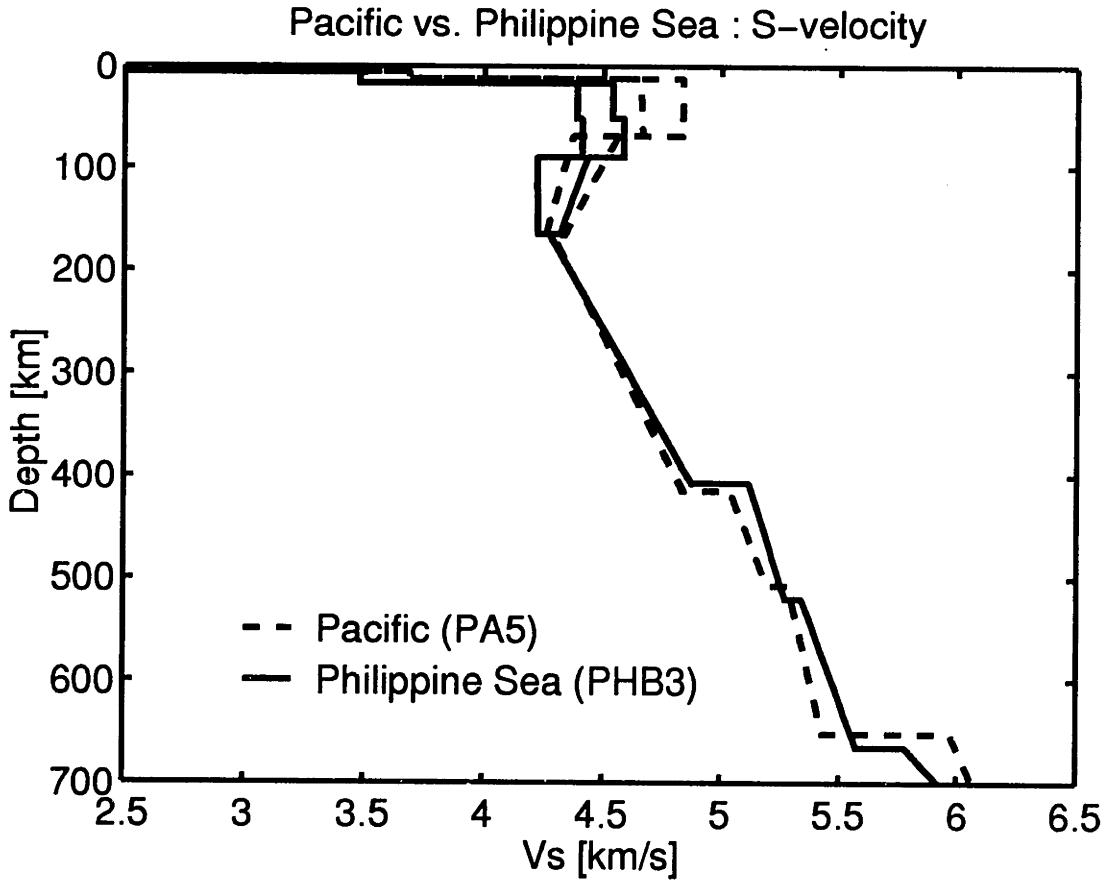
Pacific vs. Philippine Sea : S-velocity
Depth [km]
0
100
200
300
400
500
600
700
2.5
3
3.5
4
4.5
5
5.5
6
6.5
Vs [km/s]
Pacific (PA5)
Philippine Sea (PHB3)

Figure 5.1

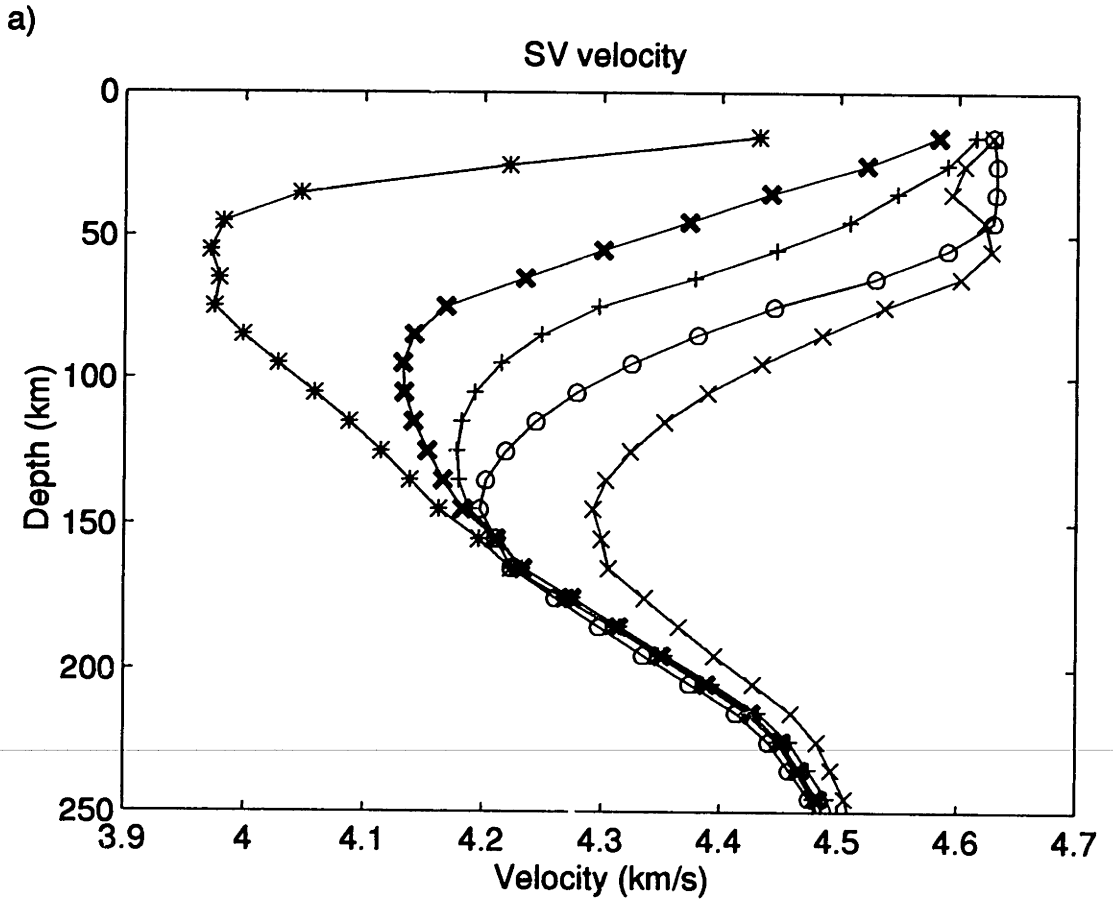
a)
SV velocity
Depth (km)
0
50
100
150
200
250
3.9
4
4.1
4.2
4.3
4.4
4.5
4.6
4.7
Velocity (km/s)

Figure 5.2a

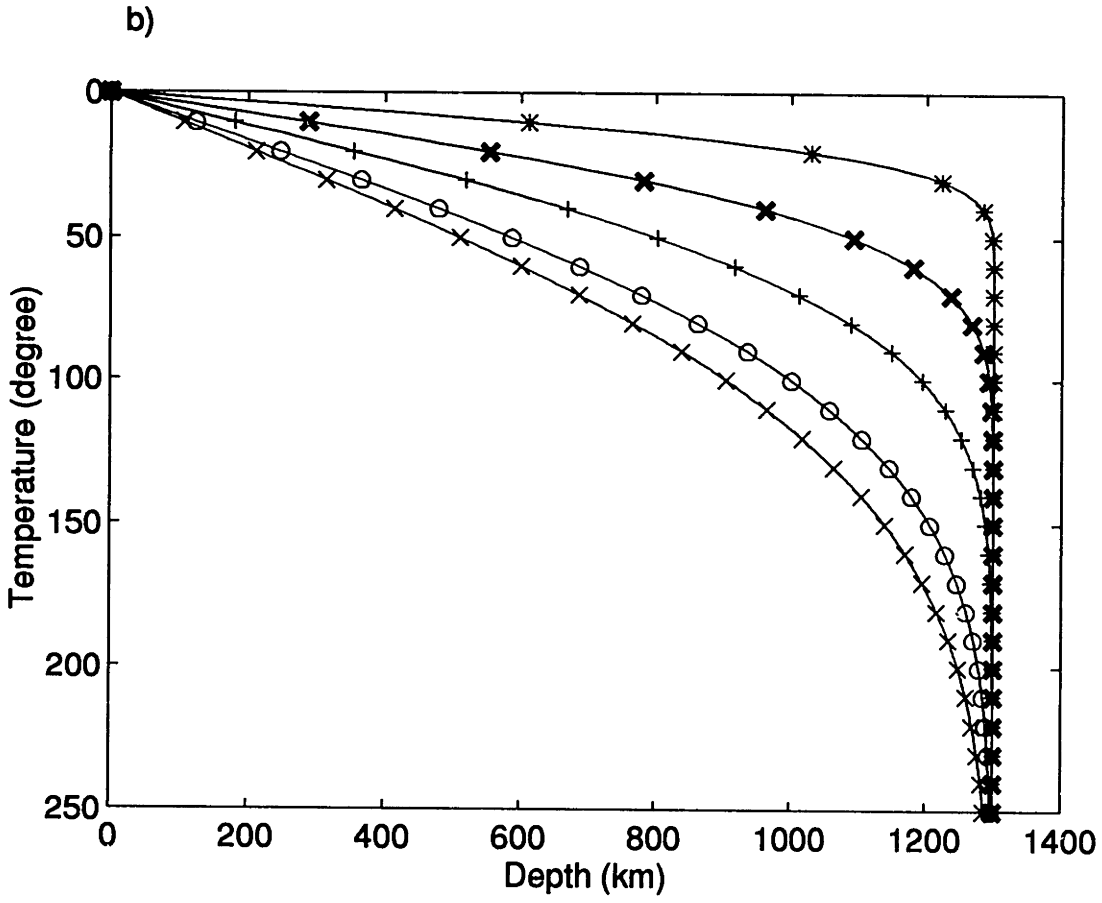
b)
0
50
100
150
200
250
Temperature (degree)
0
200
400
600
800
1000
1200
1400
Depth (km)

Figure 5.2b

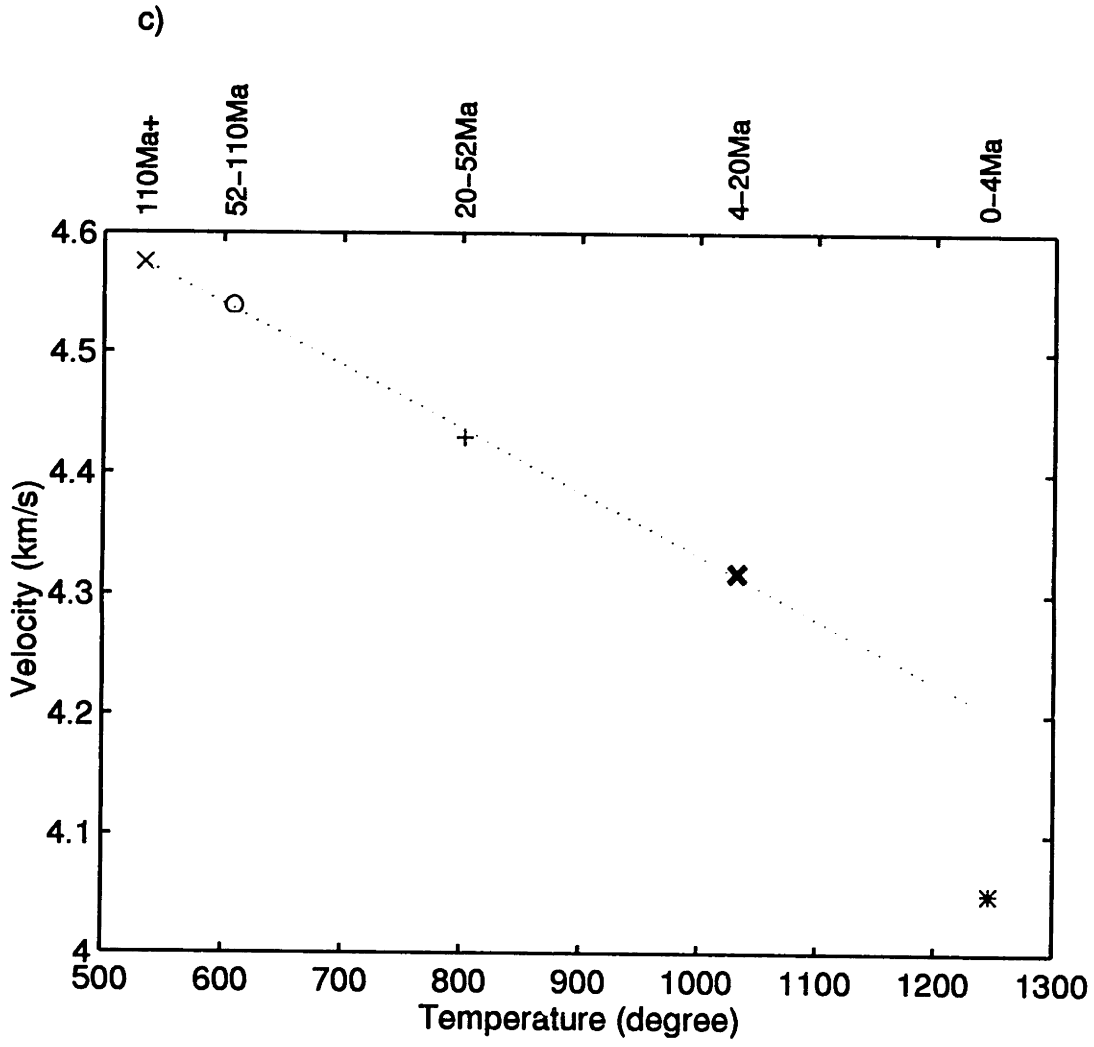
c)
110Ma+
52–110Ma
20–52Ma
4–20Ma
0–4Ma
4.6
4.5
4.4
4.3
4.2
4.1
4
Velocity (km/s)
500
600
700
800
900
1000
1100
1200
1300
Temperature (degree)

Figure 5.2c

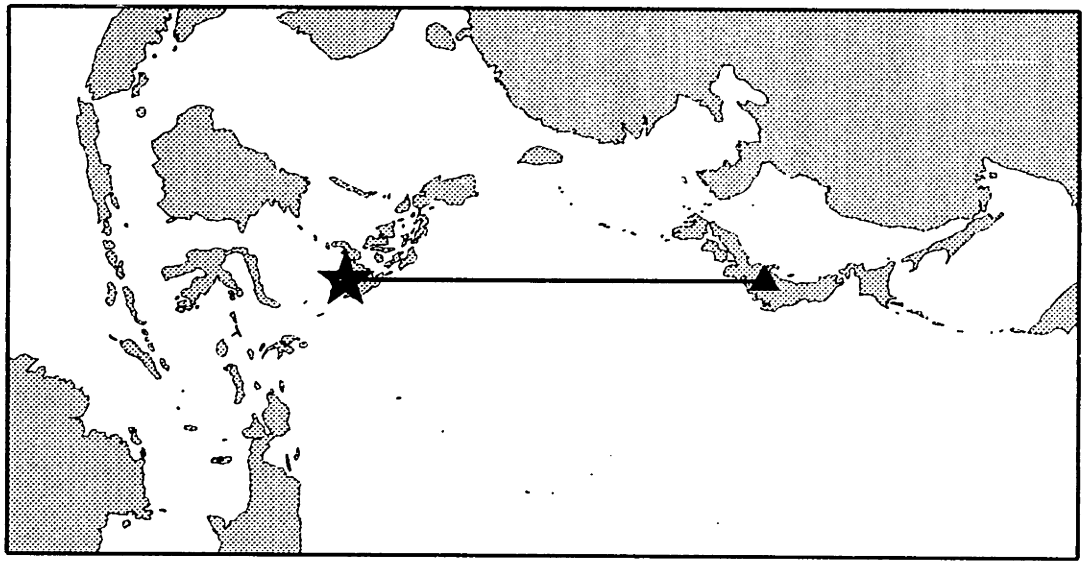

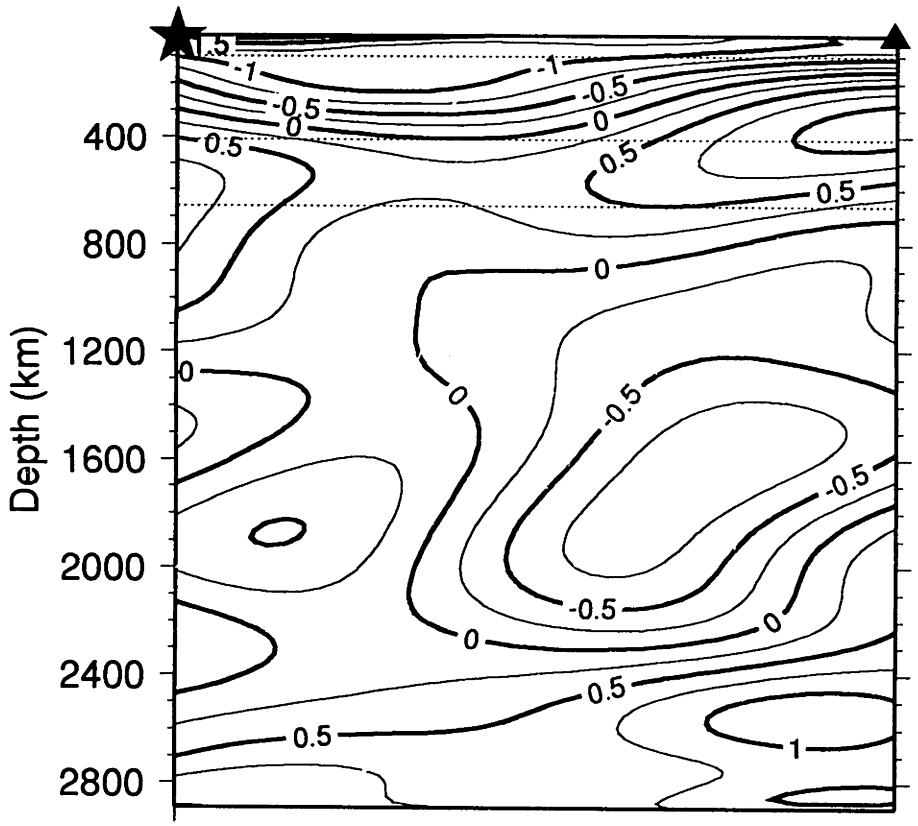

Figure 5.3

References

Anderson, D.L., *Theory of the Earth,* 366pp., Blackwell Scientific, Boston, MA, 1989.

Ben-Avraham, Z., and S. Uyeda, Entrapment origin of marginal seas, in *Geodynamics of the Western Pacific-Indonesian Region,* ed. T.W.C. Hilde, and S. Uyeda, AGU, Washington, 1983.

Cara, M., and J. J. Lévêque, Oriented olivine crystals in the upper mantle: a test from the inversion of multimode surface wave data, *Phys. Earth Planet. Int., 47,* 246-252, 1987.

Carlson, R.L., and H.P. Johnson, On modeling the thermal evolution of the oceanic mantle: An assessment of the cooling plate model, *J. Geophys. Res., 99,* 3201-3214, 1994.

Chen, W.-P., and R.L. Nowack, Constraining anomalous P-wave speeds in the mantle transition zone: Results from the Pre-POSEIDON broad-band seismic array, *EOS, 75,* 477 (Fall Meeting Supplement), 1994.

Creager, K. C., and T. H. Jordan, Slab penetration into the lower mantle beneath the Mariana and other island arcs of the northwest Pacific, *J. Geophys. Res., 91,* 3573–3589, 1986.

Dorman, J., M. Ewing, and J. Oliver, Study of shear-wave distribution in the upper mantle by Rayleigh wave, *Bull. Seism. Soc. Am., 50,* 87-115, 1960.

Dziewonski, A.M., and D.L. Anderson, Preliminary reference Earth model, *Phys. Earth Planet. Inter., 25,* 297-356, 1981.

Dziewonski, A.M., T.A. Chou, and J.H. Woodhouse, Determination of earthquake source parameters from waveform data for studies of global and regional seismicity, *J. Geophys. Res., 86,* 2825-2852, 1981.

Erdogan, N., and R.L. Nowack, Slant-stack velocity analysis for one-dimensional upper mantle structure using short-period data from MAJO, *Pure. appl. Geophys., 141,* 1-24, 1993.

Fischer, K. M., T. H. Jordan, and K. C. Creager, seismic constraints on the morphology of deep slabs, *J. Geophys. Res., 93,* 4773–4783, 1988.

Fukao, Y., M. Obayashi, H. Inoue, and M. Nenbai, Subducting slabs in the mantle transition zone, *J. Geophys. Res., 97, 4809-4822,* 1992.

Gaherty, J.B., Structure and anisotropy of the upper mantle, Ph.D. Thesis, MIT, 1995.

Gaherty, J.B., T.H. Jordan, and L.S. Gee, Depth extent of polarization anisotropy in western Pacific upper mantle, submitted to *J. Geophys. Res.,* 1996.

Gaherty, J.B., and T.H. Jordan, Lehmann discontinuity as the base of an anisotropic layer beneath continents, *Science, 268,* 1468-1471, 1995.

Gee, L.S. and T.H. Jordan, Polarization anisotropy and fine-scale structure of the Eurasian upper mantle, *Geophys. Res. Lett., 15,* 824-827, 1988.

Gee, L.S., and T.H. Jordan, Generalized seismological data functionals, *Geophys. J. Int., 111,* 363-390, 1992.

Grand, S.P. and D.V. Helmberger, Upper mantle shear structure of North America, *Geophys. J. R. astr. Soc., 76,* 399-438, 1984.

Hall, R., M. Fuller, J. Ali, and C.D. Anderson, The Philippine Sea Plate: Magnetism and reconstructions, in *Active Margins and Marginal Basins of the Western Pacific,* ed. B. Taylor, and J. Natland, AGU Geophysical Monograph 68, pp371-404, 1995.

Hirth, G., and D.L. Kohlstedt, Are the oceanic lithosphere and asthenosphere separated by a compositional boundary?, Abstract volume B, SB12C-01, IUGG, Boulder, 1995.

Inoue, H., Y. Fukao, K. Tanabe, and Y. Ogata, Whole mantle P-wave travel-time tomography, *Phy. earth Planet. Inter., 50,* 294-328, 1990.

Ita, J. and L. Stixrude, Petrology, elasticity, and composition of the mantle transition zone, *J. Geophys. Res., 97,* 6849-6866, 1992.

Jordan, T.H., Mineralogies, densities, and seismic velocities of garnet lherzolites and their geophysical importance, in *The Mantle Sample: Inclusions in Kimberlites and Other Volcanics,* ed. F.R. Boyd and H.O.A. Meyer, pp 1-14, AGU, Washington, D.C., 1979.

Kanamori, H. and K. Abe, Deep structure of island arcs as revealed by the surface waves, *Bull. Earthquake Res. Inst. Univ. Tokyo, 86,* 1001-1025, 1968.

Karato, S.-I., Does partial melting reduce the creep strength of the upper mantle?, *Nature, 319,* 309-310, 1986.

Karato, S.-I., Effect of water on seismic wave velocities in the upper mantle, *Proc. Japan Academy, 71,* Ser B.61-66, 1995.

Karato, S.-I., S.S. Peterson, and J.D. Fitz Gerald, Rheology of synthetic olivine aggregate: Influence of grain size and water, *J. Geophys. Res., 91,* 8151-8176, 1986.

Kato, M., and T.H. Jordan, Upper mantle structure beneath the western Philippine sea from body waves, surface waves and ScS reverberations, *EOS Trans. AGU, 75,* 477, 1994..

Katzman, R., and T.H. Jordan, Seismic tomography using *ScS* reverberations, Abstract volume B, SB41E-08, IUGG, Boulder, 1995.

Lévêque, J.-J., and Cara, M., Inversion of multimode surface wave data: evidence for sub-lithospheric anisotropy, *Geophys. J. R. astr. Soc., 83,* 753-773, 1985.

Lerner-Lam, A.L. and T.H. Jordan, How thick are the continents?, *J. Geophys. Res., 92,* 14007-14026, 1987

Li, X.-D., and T. Tanimoto, Waveform inversion of long-period seismic data for structure, in *Seismic Tomography: Theory and Practice,* eds. H.M. Iyers and K. Hirahara, pp 64-91, Chapman and Hall, London, 1993.

Louden, K.E., The crustal and lithospheric thickness of the Philippine Sea as compared to the Pacific, *Earth Planet. Sci. Lett., 50,* 275-288, 1980.

Mammerickx, J., R.J. Fisher, F.J. Emmel, and S.M. Smith, Bathymetry of the East and Southeast Asian Seas ,in *Geophysical Atlas of East and Southeast Asian Seas,* ed. D.E. Hayes, Geol. Soc. Am. Map Series MC-25, 1978.

Maupin, V., Partial derivatives of surface-wave phase velocities for flat anisotropic models, *Geophys. J. R. astr. Soc., 83,* 379-398, 1985.

McKenzie, D.P., Some remarks on heat flow and gravity anomalies, *J. Geophys. Res., 72,* 6261-6273, 1967.

McNutt, M.K., and A.V. Judge, The Superswell and mantle dynamics beneath the South Pacific, *Science, 248,* 969-975, 1990.

McNutt, M.K., Marine geodynamics: Depth-age revisited, *Rev., Geophys., Supple.,* 413-418, 1995.

Mrozowski, C.L., and D.E. Hayes, Sediment isopachs, in *Geophysical Atlas of East and Southeast Asian Seas,* ed. D.E. Hayes, Geol. Soc. Am. Map Series MC-25, 1978.

Murauchi, S., N. Den, S. Asano, H. Hotta, T. Yoshii, T. Asanuma, K. Hagiwara, K. Ichikawa, T. Sato, W.J. Ludwig, J.I. Ewing, N.T. Edger and R.E. Houtz, Crustal structure of the Philippine Sea, *J. Geophys. Res., 73,* 3143-3171, 1968.

Nakanishi, I., Surface wave tomography: velocity and Q, in *Seismic Tomography: Theory and Practice,* eds. H.M. Iyers and K. Hirahara, pp 92-132, Chapman and Hall, London, 1993.

Nishimura, C.E., and D.W. Forsyth, The anisotropic structure of the upper mantle in the Pacific, *Geophys. J. Int.,* 96, 203-229, 1989.

Nolet, G., Imaging the upper mantle with partitioned non-linear waveform inversion, in *Seismic Tomography: Theory and Practice,* eds. H.M. Iyers and K. Hirahara, pp 248-264, Chapman and Hall, London, 1993.

Oda, H., and N. Senna, Regional variation in surface wave group velocities in the Philippine Sea, *Tectonophys., 233,* 265-277, 1994.

Park, C.-H., K. Tamaki, and K. Kobayashi, Age-depth correlation of the Philippine Sea back-arc basins and other marginal basins in the world, *Tectonophys., 181,* 351-371, 1990.

Parsons, B., and J.G. Sclater, An analysis of the variation of the ocean floor bathymetry and heat flow with age, *J. Geophys. Res., 82,* 803-827, 1977.

Peacock, S.M., Fluid process in subduction zone, *Science, 248,* 329-337, 1990.

Regan, J., and D. L. Anderson, Anisotropic models of the upper mantle, *Phys. Earth Planet. Int., 35,* 227-263, 1984.

Revenaugh, J. and T.H. Jordan, Observation of first-order mantle reverberations, *Bull. Seis. Soc. Am., 77,* 1704-1717, 1987.

Revenaugh, J. and T.H. Jordan, Mantle layering from ScS reverberations, 1. Waveform inversion of zeroth-order reverberations, *J. Geophys. Res., 96,* 19,749-19,762, 1991a.

Revenaugh, J. and T.H. Jordan, Mantle layering from ScS reverberations, 2. The transition zone, *J. Geophys. Res., 96,* 19,763-19,780, 1991b.

Revenaugh, J. and T.H. Jordan, Mantle layering from ScS reverberations, 3. The upper mantle, *J. Geophys. Res., 96,* 19,781-19,810, 1991c.

Revenaugh, J. and T.H. Jordan, Mantle layering from ScS reverberations, 4. The Lower mantle and core-mantle boundary, *J. Geophys. Res., 96,* 19,811-19,824, 1991d.

Ringwood, A.E., *Composition and Petrology of the Earth's Mantle,* 604 pp., McGraw-Hill, New York, 1975.

Sato, H., I.S. Sacks, and T. Murase, The use of laboratory velocity data for estimating temperature and partial melt fraction in the low-velocity zone: Comparison with heat flow and electrical conductivity studies, *J. Geophys. Res., 94,* 5689-5704, 1989.

Sclater, J. G., D. Karig, L. A. Lawver, and K. Louden, Heat flow, depth, and crustal thickness of the marginal basins of the south Philippine Sea, *J. Geophys. Res., 81,* 309-318, 1976.

Seekins, L.C. and T. Teng, Lateral variations in the structure of the Philippine sea plate, *J. Geophys. Res., 82,* 317-324, 1977.

Seno, T., Age of subducting lithosphere and back-arc basin formation in the western Pacific since the Middle Tertiary, in *Formation of Active Ocean Margins,* ed. N. Nasu et al., Terrapub, Tokyo, 1985.

Seno, T. and S. Maruyama, Paleogeographic reconstruction and origin of the Philippine sea, *Tectonophys., 102,* 53-84, 1984.

Shearer, P.M, Global mapping of upper mantle reflectors from long-period *SS* precursors, *Geophys. J. Int., 115,* 878-904, 1993.

Shearer, P.M., and T. G. Masters, Global mapping of topography on the 660-km discontinuity, *Nature, 355,* 791-796, 1992.

Sheehan, A.F., and S.C. Solomon, Joint inversion of shear wave travel time residual and geoid and depth anomalies for long-wavelength variations in the upper mantle temperature and composition along the mid-atlantic ridge, *J. Geophys. Res., 96,* 19,981-20,009, 1991.

Shimamura, H., Y. Tomoda, and T Asada, Seismographic observation at the bottom of the central basin fault of the Philippine Sea, *Nature, 253,* 177-179, 1975.

Shiono, S, I. S. Sacks, and A.T. Linde, Preliminary velocity structure of Japanese islands and Philippine sea from surface wave dispersion, *Carnegie Inst. Washington Yearbook, 79,* 498-505, 1980.

Stein. C., and S. Stein, A model for the global variation in oceanic depth and heat flow with lithospheric age, *Nature, 359,* 123-129, 1992.

Su, W.-J., R.L. Woodward, and A.M. Dziewonski, Degree 12 model of shear velocity heterogeneity in the mantle, *J. Geophys. Res., 99,* 6945-6980, 1994.

Tajima, F., and S. Grand, Evidence of high velocity anomalies in the transition zone associated with southern Kuril subduction zone, *Geophys. Res. Lett., 23,* 3139-3142, 1995.

Tamaki,. K., and E. Honza, Global tectonics and formation of marginal basins: Role of the western Pacific, *Episodes, 14,* 224-230, 1991.

Tanimoto, T., Waveform inversion of mantle Love waves: the Born seismogram approximation, *Geophys. J. R, astr. Soc., 93,* 321-334, 1984.

Tarantola, A. and B. Valette, Generalized nonlinear inverse problems solved using the least squares criterion, *Revs. Geophys. Space Phys., 20,* 219-232, 1982.

Taylor, B., and G.D. Karner, On evolution of marginal basins, *Rev. Geophys. Space. Sci., 21,* 1727-1741, 1983.

Turcotte, D.L., and E.R. Oxburgh, Finite amplitude convection cells and continental drift, *J. Fluid Mech., 28,* 29-42, 1967.

van der Hilst, R.D., R. Engdahl, W. Spakman, and G. Nolet, Tomographic imaging of subducted lithosphere below northwest Pacific island arcs, *Nature,* 353, 37-43, 1991.

van der Hilst, R.D., and T. Seno, Effect of relative plate motion on the deep structure and penetration depth of slabs below the Izu-Bonin and Mariana islands arc, *Earth Planet. Sci. Lett. 120,* 395-407, 1993.

van Heijst, H.J., R. Snieder, and R. Nowack , Resolving a low-velocity zone with surface wave data, *Geophys. J. Int., 118,* 333-343, 1994.

Watts, A.B., and J.H. Bodine, Free-Air Gravity, in *Geophysical Atlas of East and Southeast Asian Seas*, ed. D.E. Hayes, Geol. Soc. Am. Map Series MC-25, 1978.

Wessel, P. and W.H.F. Smith, Free software helps map and display data, *EOS Trans. Amer. Geophys. U., 72,* 441, 445-446, 1991.

Woodhouse, J.H., and A.M. Dziewonski, Mapping the upper mantle: three-dimensional modeling of the earth structure by inversion of seismic waveforms, *J. Geophys. Res., 89,* 5953-5986, 1984.

Yu, Y., and J. Park, Hunting for azimuthal anisotropy in the Pacific Ocean region, *J. Geophys. Res., 99,* 15, 399- 15, 422, 1994.

Zielhuis, A., and G. Nolet, Shear-wave velocity variations in the upper mantle beneath central Europe, *Geophys. J. Int., 117,* 695–715, 1994.

Zhang, Y.-S. and T. Tanimoto, High-resolution global upper mantle structure and plate tectonics, *J. Geophys. Res., 98,* 9793-9823, 1993.

Acknowledgment

There are many people to whom I am grateful for making my stay at MIT a positive and fruitful experience.

First of all, I'd like to thank Tom Jordan for being an excellent advisor. He made me realize that seismology is only a subset of Earth science, and geophysics is just a small piece of physics. I just simply admire his deep insight, his instinct for a new direction, and his love for hot food.

Brad Hager gave me an opportunity to get an acquaintance with the world of geodynamics. Chris Marone's classes have been the best classes I ever had attended, and I respect his eagerness for interacting with students.

Jim Gaherty has been my *de facto* advisor from start to finish. Without his knowledge and experience of the GSDF methodology, this project could not be completed. No doubt in my mind that he will become a very good teacher and hopefully this will happen soon. Special thanks to Lind Gee for her contribution on GSDF and many other compute codes, which have been vital in my project.

People of the 5th floor have created a supportive environment, and have taught me many things you needed to know as a graduate student. I am grateful to Susan Evans, Nic Fiszman, Paolo Harabaglia, Pierre Ihmlè, Rafi Katzman, Sang-Mook Lee, Pat McGovern, Jeff McGuire, Nori Namiki, Peter Puster, Mark Simons, and Li Zhao for sharing the love for coffee and newspaper. I am specially grateful to my office mates: Jim, Susan, Sang-Mook, Rafi, and Jeff. I have been the only single student both in room 526 and 522, and they (and their spouses and children) provided me an opportunity to learn a little bit of how to live a married life.

Dave Krowitz, Linda Meinke, Dave Bauman, and Mike Batchelder have kept the computer running. Many thanks to Libby Kurten, Marie Sénat, Deb Sykes, Darla Smutka for helping me through the paperwork. Special thanks to Beverly Kozol-Tattlebaum, whose "*Hi, How are you?*" is one of my most pleasant memories at MIT. She was the first person I met when I visited MIT, and ever since has been sending me a beautiful smile.

I am grateful to my advisors at Kyoto University, Takeshi Mikumo, Kazuro Hirahara, and Masataka Ando for supporting my decision to come to MIT, to Tommy Iwata, and Keiko Kuge for their encouragement. My friends in Japan have kept me posted on everything, from gossips to politics, through the Information Superhighway, and I am thankful for all of them.

Finally, I will always be thankful for my family for all of their support. Frequent phone conversations with my sister Chizuru (who finally learned how to use e-mail) reminded me that I was not alone. She asked me many new questions ranging from biology to economics, and I hope my answers have helped her earn good grades. My Mom and Dad have been always supportive since they first showed me the city of Cambridge when I was 3 and was speaking French (though, my Boston experience has not been as sweet as *Love Story*, Mom). This is a family full of love, and *Love means never having to say you're sorry*. Thank you all.